CRWR Online Report 10-03

Hydraulic Performance of Temporary Construction Traffic Barriers

by

Cody Brent Hudson, B.S.

Randall J. Charbeneau, Ph.D.

Michael E. Barrett, Ph.D.

May 2010

Center for Research in Water Resources

The University of Texas at Austin

J.J. Pickle Research Campus

Austin, TX 78712-4497

This document is available online via the World Wide Web at

http://www.crwr.utexas.edu/online.shtml

Acknowledgements

This research was funded by the Texas Department of Transportation under project number 0-6094, “Mitigation Methods for Temporary Concrete Traffic Barrier Effects on Flood Water Flows”.

Abstract

Temporary Concrete Traffic Barriers (TCTBs) are essential in order to protect the traveling public and highway construction crews from accidents due to driver misfortune or negligence. In order for TCTBs to be installed, however, they must be successfully crash tested. Barrier height and drainage open space are key characteristics that influence this crash test rating. This is because an increase in height will insure that a vehicle will not overtop the barrier and a decrease in drainage open space will result in greater barrier mass, which will in turn resist larger impact forces. The factors that increase the crash worthiness of a barrier, however, lead to poor hydraulic performance. This then becomes a concern if barriers are placed in areas where they may adversely impact the local floodplain elevation. The objective of this research is the development of a hydraulic rating curve that describes the relationship between upstream energy head and the flow rate passing the barrier. To accomplish this objective, a three parameter model with three unknown coefficient terms was utilized. The model was then fit to experimentally obtained data, and a rating curve was developed. In addition, the effects of downstream submergence and clogging of the drainage opening, with respect to the rating curve, was also analyzed. Finally, a method for using this information in the hydraulic modeling software HEC-RAS was developed.

Table of Contents

List of Tables

List of Figures

Chapter One

Introduction

1.1 PROBLEM DESCRIPTION

Temporary Concrete Traffic Barriers (TCTBs) are essential in order to protect the traveling public and highway construction crews. They are rigid barricades that help prevent accidents due to driver misfortune or negligence. However, for these barriers to maximize crash safety, some properties such as hydraulic capacity become diminished. This is because larger drain openings that would increase the hydraulic capacity result in a decrease in the barrier weight and/or a higher center of gravity, which increases the barrier's susceptibility to overturning when impacted. However, smaller openings can result a higher water elevation upstream of the barrier, which in turn can increase the local floodplain elevation. It is therefore paramount that the balance between barrier stability and hydraulic performance be optimized. The hydraulic performance of four barriers is the focus of this report. In particular, this research focuses on development of a hydraulic rating curve that models the relationship between flow and upstream energy and how downstream submergence and clogging will affect this relationship. Finally, with this information, a method was developed by which a more precise evaluation of the impacts of barrier placement could be determined using HEC-RAS.

1.2 OBJECTIVES

The objectives of this research are as follows:

1) Develop rating curves for four standard type TCTBs.
2) Model the effect that downstream submergence will have on the rating curves.
3) Evaluate the effect of clogging.
4) Develop a procedure by which barrier placement can be modeled in the hydraulic modeling software HEC-RAS.

In order to accomplish the first objective, a three parameter model developed by Charbeneau et al. (2008) was utilized. To accomplish the second task two models were used. The first, by Villemonte (1947), was developed in order to describe the effects that downstream submergence will have on a weir, but has proven to model barriers with small drainage openings quite well. Also, a model developed by Charbeneau et al. (2008) will be employed by which the Villemonte model was adapted to account for larger drainage openings. For the third task, a procedure was developed during this research by which a model barrier was fitted with a device that allowed for testing the barrier with different amounts of clogging. Finally, for objective four, two example problems in HEC-RAS were used to demonstrate the effects of barrier placement on the local floodplain elevation. These methods differ from previous modeling alternatives which included increasing the roadway elevation to simulate a solid barrier.

Chapter Two

Literature Review

2.1 INTRODUCTION

The foundation for this study is based on several key principles from fluid mechanics. This section will review principles including the energy equation, specific energy/critical flow, and the equations for flow over a weir and through an orifice, in order to provide a starting point for explaining the models that were developed in this research.

2.2 GENERAL ENERGY EQUATION

In order to understand how phenomenon in the environment work, a study of the energy in a system is generally conducted. This is because the law of conservation of energy allows for the development of equations that can predict future outcomes based on changes in energy states. One such relationship is the General Energy Equation for open channel flow (Equation 2.1). This equation is an adaptation of Bernoulli's Equation that accounts for a non-uniform flow distribution (α) and energy lost to heat (h_L), due to friction, between locations 1 and 2. Other key terms in the equation are as follows: z (vertical distance from constant datum), h (liquid depth), v (velocity), and g (gravitational constant), where the subscript denotes locations 1 and 2.

$$z_1 + h_1 + \alpha_1 \frac{v_1}{2g} - h_L = z_2 + h_2 + \alpha_2 \frac{v_2}{2g} \qquad (2.1)$$

However, several simplifying assumptions can be made that greatly reduce the complexity of this equation. The following simplifications to Equation 2.1 were presented by Klenzendorf, 2007. First of all, z_1 and z_2 can be omitted, because the slope in the test channel is approximately zero, which makes these terms equal. Also, if a uniform flow distribution is assumed, due to a negligible effect by the channel walls and bottom, α can also be omitted because it would approximately equal a value of 1. The result of these assumptions is then given by Equation 2.2, given below, in which E is the specific energy.

$$E_1 = h_1 + \frac{{v_1}^2}{2g} = h_2 + \frac{{v_2}^2}{2g} = E_2 \tag{2.2}$$

Next, it is then possible using the volumetric flow rate equation, Q=Av, to solve for the velocity term. In this equation Q (volumetric flow rate) is equal to the v (velocity) of the liquid times the A (area) that the water is flowing through. Since the geometry of the channel is known and the height and flow of the water are being measured, it is then possible to calculate the energy. Equation 2.3, located below, shows this result, where E (energy) is related to the h (liquid depth) and Q (volumetric flow rate).

$$E = h + \frac{Q^2}{2gA^2} \tag{2.3}$$

Lastly, one more change is necessary, which allows for the calculation of flow on a per linear foot basis. This step allows an easy calculation to be performed for determining the flow rate that is associated with varying lengths of barrier. The variable q (unit flow rate) is then defined as Q (volumetric flow rate) divided by b (channel width), or q=Q/b. Substituting this change into Equation 2.3, then results in Equation 2.4 listed

below, which is the form of the energy equation used for this research, where some further simplification has also been accomplished given that A (area) equals b (channel width) times h (liquid depth).

$$E = h + \frac{q^2}{2gh^2} \tag{2.4}$$

2.3 SPECIFIC ENERGY AND CRITICAL FLOW

As it was developed in the last section in Equation 2.2, the energy of a fluid in an open channel can be calculated if the height and velocity of a fluid are known. Figure 2.1 below, shows the specific energy associated with a varying water depth. There are several key features in this figure. First, the line E=h corresponds to the potential energy that would occur if the fluid was stagnant. This is important because it means that the horizontal distance from the y axis to this line represents the value of the h term in Equation 2.2, and the remaining distance from the E=h line to the curve is the resulting kinetic energy ($v^2/2g$). Secondly, it can be seen from the graph that two different water depths can result in equivalent quantities of energy. It is then useful to be able to name the type of flow that is associated with each energy condition. A clear breaking point between the potential energy dominated flow regime and the kinetic energy dominated flow regime is the critical point. This point is the minimum specific energy that can be developed for a given channel discharge and is calculated by taking the derivative of the specific energy with respect to depth, dE/dh, and setting the resulting equation equal to zero. Solving this equation for depth results in the value for the critical depth, h_c, and is shown below in Equation 2.5. Points on the graph greater than the critical depth are called subcritical and points less than the critical depth are called supercritical.

$$h_c = \left(\frac{q^2}{g}\right)^{1/3} \tag{2.5}$$

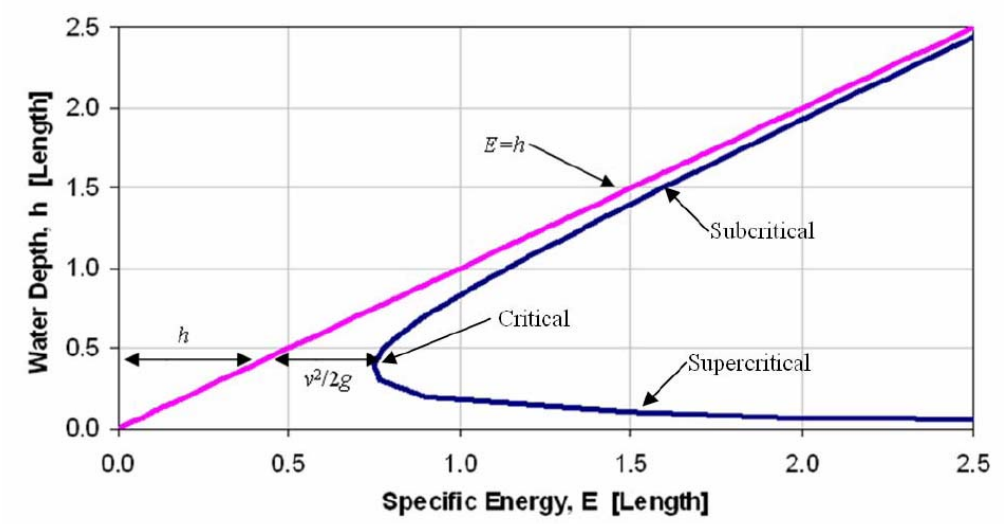

Figure 2.1 – Specific Energy Graph

The critical depth is important for the development of a mathematical model used in developing a rating curve for this research. If it is assumed that water flowing through an obstruction (i.e., a TCTB) causes the water to pass through a critical state at or near the obstruction, a relationship between the critical height and a measured height upstream can be developed using the general energy equation and Equation 2.5. This is illustrated below in Equation 2.6, in which the subscript c indicates the critical location near the TCTB and the subscript u indicates the location upstream where the water level height is being recorded.

$$h_c + \alpha_c \frac{{v_c}^2}{2g} - h_L = h_u + \alpha_u \frac{{v_u}^2}{2g} \tag{2.6}$$

However, additional assumptions can also be made that will further simplify the equation. First, the upstream flow will be subcritical due to the TCTB obstruction. This will cause the upstream kinetic energy part of the equation to be negligible when compared to the potential energy or $\frac{{v_u}^2}{2g} \ll h_u$. Secondly, as previously mentioned in Section 2.2, the α and h_L terms can be neglected. Lastly, if v_c is converted into an equivalent expression with q (unit flow) as was done in Section 2.2, we obtain Equation 2.7, which is listed below.

$$h_c + \frac{q^2}{2g{h_c}^2} = h_u \tag{2.7}$$

Next, if Equation 2.5 is rearranged and solved for q^2, the result is $q^2 = g{h_c}^3$. If this is then substituted into Equation 2.7 and rearranged to solve for h_c, an equation is developed which gives the critical depth as a function of upstream depth. This equation is given below as Equation 2.8.

$$h_c = \frac{2}{3} h_u \tag{2.8}$$

This equation is especially helpful for the development of a mathematical model, which approximates the rating curve data gathered for each barrier type. Since, the actual value of the critical depth cannot be measured, this relationship allows for the calculation of the transition point, between supercritical to subcritical, with the measured data upstream of the model.

2.4 GENERAL FLOW EQUATIONS

2.4.1 Weir Flow

Several different methods can be used to measure the flow of a liquid, such as venturi tubes, turbine flowmeters, magnetic flowmeters, pitot tubes, and weirs. The method used in this research is the weir. A weir is a barrier or dam placed in the channel so that the fluid backs up behind it then falls through a notch cut into the face of the weir (Mott, 2000). For specifications concerning the particular weir used to measure flow in this research, see Section 3.3.3. The weir equation will also be useful when deriving the model equations describing the flow over a barrier, and will be discussed more in Section 4.2.3.

The general equation for weirs with horizontal crests is given by the following equation (King & Brater, 1963):

$$Q = Cbh_w{}^n \tag{2.9}$$

In this equation Q is the volumetric flow rate, C is the weir coefficient derived for each specific weir, b is the width of the weir, h_w is the height of the water above the weir crest, and n is dependent on the weir geometry. The weir equation in this research is used both in the calculation of flow for the development of a rating curve and in deriving the model used to describe the flow over the barrier. For measuring the flow rate during the experiments a more specific form of the weir equation is used, which was developed to model the flow over sharp crested rectangular weirs and is given below in Equation 2.10 (Rouse, 1950). In this equation C_d is an empirically derived weir coefficient that is

dependent on the effects of viscosity, the velocity distribution and capillarity (Rouse, 1950) , and all other terms have been defined previously.

$$Q = C_d \frac{2}{3} b\sqrt{2g} h_w^{1.5} \quad (2.10)$$

2.4.2 Orifice Flow

In addition to the weir equation, the orifice flow equation is useful in the development of the model used in this research. According to King & Brater (1963), an orifice is a restricted opening with a closed perimeter through which water flows. The flow rate through a sharp crested orifice (the type of orifice that the barriers possess) is described by Equation 2.11, which is given by Bos (1989).

$$Q = C_d A_o \sqrt{2gh_o} \quad (2.11)$$

In this equation, C_d is a unitless discharge coefficient, A_o is the cross-sectional area of the orifice, h_o is the upstream head acting on the centroid of the orifice area, and Q and g have been defined previously.

Equation 2.11, however, is only valid when h_o is greater than the height of the orifice opening, and the discharge is unrestricted downstream. When the orifice becomes submerged upstream and downstream a slight alteration to this equation is necessary. The equation governing submerged orifice flow is also given by Bos (1989) and is shown below as Equation 2.12, where Δh_o is the difference in upstream and downstream head acting on the centroid of the orifice.

$$Q = C_d A_o \sqrt{2g\Delta h_o} \quad (2.12)$$

Chapter Three

Physical Setup and Methodology

3.1 INTRODUCTION

The purpose of this report is the development of rating curves that will predict the hydraulic performance of the: Single Slope Concrete Barrier (SSCB), Single Slope Concrete Barrier SPL (SSCBSPL), Concrete Safety Barrier (CSB) and Low Profile Concrete Barrier (LPCB). To accomplish this, physical modeling was performed at the Center for Research in Water Resources (CRWR) on the J.J. Pickle Research Campus in Austin, TX. The remaining sections will cover the construction of the models, the layout of the testing facility, and the methods used in data collection.

3.2 MODEL CONSTRUCTION

The first step in this experiment was the construction of the model and model base. This was a key step because the quality of the models being tested will inevitably affect the quality of the results. The next two sections will discuss the process involved and the decisions that were made during construction.

3.2.1 TCTB Model Construction

The models were constructed using TxDOT standard drawings, which are included in Appendix A. These drawings were obtained from the TxDOT website (TxDOT, 2009), and are available to the public. For the construction of the models, timber was chosen as an alternative to concrete (actual barrier material), because of the

relative ease of construction and movement, and because the hydraulic properties being measured are independent of the material, as long as the material is impermeable. In order to make the models as impermeable as possible, all the pieces were coated twice with a water proofing compound and with a final coat of primer paint. This also assured that the models would not warp or disintegrate during multiple tests. As seen in Figures 3.1-3.3, the models were constructed with a hollow interiors and open ends to decrease the effect of buoyancy forces during testing. This, however, will have little effect on the hydraulic properties being tested, because testing is only conducted after the flow has reach steady state, and under these conditions the amount of water flowing into and out of the model is negligible compared to the total amount of flow. Furthermore, in order for the models to conform to the existing test channel at the CRWR, the models were constructed at half scale with only half of a typical barrier section and one scupper drain analyzed. Lastly, only one model barrier was constructed to analyze both the SSCB and SSCBSPL. This is because both barriers had similar geometries with different sized drainage openings. This model will be referred to as the Modified Single Slope Concrete Barrier (MSSCB). Through adaptations to this model both the SSCB and SSCBSPL barrier's rating curves were developed.

Figure 3.1 – MSSCB Model

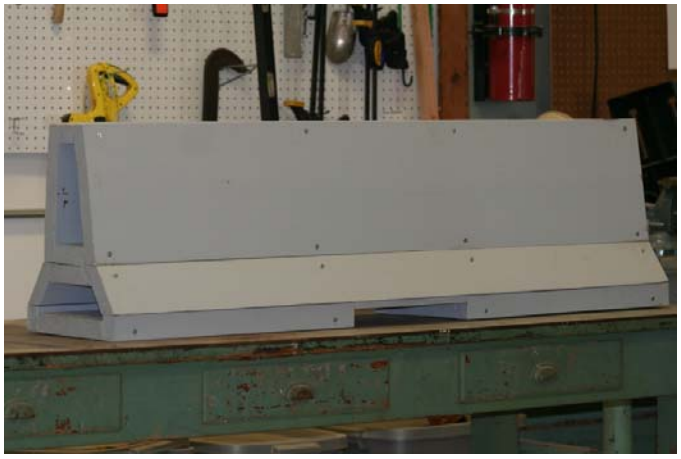

Figure 3.2 – CSB (1) - 4 Model

Figure 3.3 – LPCB (1) – 92 Model

3.2.2 TCTB Descriptions

Temporary Concrete Traffic Barriers (TCTBs) are used in order to prevent traffic from leaving the main driving surface. They are placed in locations where protection from oncoming traffic is needed and to provide safety for work crews in construction areas. The most important factor in determining the hydraulic performance of a TCTB is the drainage opening size. Some of the parameters, which affect this performance, such as height of barrier (h_r), height of drain opening (h_{rl}), width of drain opening (b_{rl}), and F_o (Fraction of open space) for the model barriers are included below in Table 3.1. For a more detailed examination of the actual barrier dimensions, see the standard drawings in Appendix A.

Table 3.1 – Key TCTB Model Parameters

TCTB-Model	h_r (in.)	h_{rl} (in.)	b_{rl} (in.)	F_o (%)
MSSB	21	6	8	3.81
CSB	16.5	1.5	12	1.82
LPCB	10	1	12	2.00

3.2.3 Model Support Construction

Before construction of the models began, a support base was constructed in the channel to firmly anchor the models during testing. Since previous experiments completed in the channel were successful with a particular base design, it was decided that a similar base should be constructed. The outside dimensions of the base are as follows: five feet (152cm) along the width of the channel, four feet (122 cm) along the length of the channel, and approximately 6 1/2 inches (16.2 cm) in height from the channel bottom. For the construction of the base 2x6 boards, 5/8 inch (1.6 cm) thick plywood, concrete, and sand were utilized. Figure 3.2, looking downstream in the channel, shows the model support base before being sealed with the top plywood piece.

The base was constructed with two sections. The upstream section was filled with concrete and has inside dimensions of 4.5 feet (137 cm) along the width of the channel, one foot (31 cm) along the length of the channel, and approximately five inches (13 cm) from the channel bottom. The concrete was utilized to provide the rigidity needed for the three support bars, located in the middle of the base and at nine inches (30 cm) from each side of the channel. The downstream section was filled with sand to give the base more mass, in order to resist the forces experienced during testing. Also, the three boards perpendicular to the direction of flow were each fitted with two brackets that were anchored to the bottom of the channel. Two boards were also added on the outside of the main frame and were not connected to the frame or the channel. Theses boards would allow the release of water upstream of the base after completion of testing, and were held in place with brackets connected to the base and the channel walls on the downstream side of the base.

Figure 3.2 – Support Base without Plywood Top

3.3 TESTING FACILITY LAYOUT

The laboratory setup at CRWR consists of: a reservoir, two pumps with valves to regulate flow, a main channel (where the model is located), the return channel, and a sharp crested weir located in the return channel upstream from the reservoir (used to measure flow). A visual diagram, Figure 3.3, is presented below to better explain the layout. In addition to these items, components used in this experiment include: nine pitot tubes connected to an inclined manometer board, which is used for measuring the height of the water upstream and downstream of the model, and a tail water gate located in the main channel that was used to increase the water elevation downstream of the model. Each of the components listed above will be described in more detail in the subsequent sections.

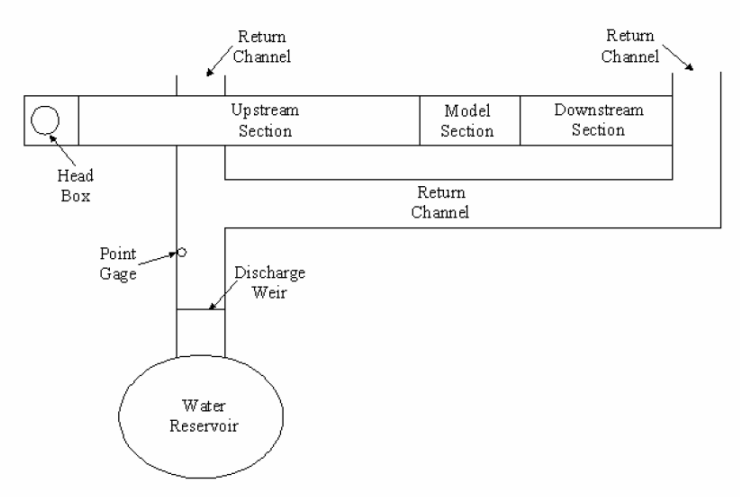

Figure 3.3 – Testing Facility Layout (Klenzendorf, 2007)

3.3.1 Water Delivery System

The water used in testing is stored in a half million gallon capacity reservoir, which has to be periodically filled due to loss from evaporation and leakage. Two centrifugal pumps are located in the reservoir and are used to move the water to the main testing channel. Each pump can be operated independently and is fitted with a valve which allows the flow in the channel to be adjusted. The water from the pumps enters a head box (see Figure 3.4) which is located at the start of the main channel, and is fitted with several devices that dissipate and distribute the flow of the incoming water, so that the flow upstream of the model is relatively uniform. The first of these devices is a collection of 3.5 in (9cm) pall rings used to reduce energy. The pall rings are followed by a partition of concrete cinder blocks, which further decrease the energy. These devices are then finally followed by nine baffle plates that are spaced approximately 6 in (15 cm)

apart and are 5 ft (152 cm) in length, which distribute the flow across the width of the channel.

Figure 3.4 – Head Box

The water then flows down the main channel where the testing equipment and model are located. At the end of the main channel the water then falls into the return channel which is at an elevation of approximately 3 feet (91cm) below that of the test channel. Due to the fact that another testing locale uses the same return channel the water then flows two ways, however, all the water used is routed back to the reservoir, where it must first flow over sharp crested weir. Therefore, no water is lost during testing and flow measurements, using the sharp crested weir, can be recorded once the system has reached steady state conditions.

3.3.2 Channel Description

The main channel, where the model is located, is approximately 125 feet (38.1 m) in length, 5 feet (152cm) in width, and two feet eight inches (81cm) in height. The slope of the channel is approximately horizontal (zero slope) and the sides are approximately perpendicular to the bottom. The upstream face of the model is located approximately 90 feet (27.4 m) from the start of the channel. The two sets of pitot tubes upstream of the model are at locations 75 feet (22.9 m) and 80 feet (24.4 m) from the start of the channel and the downstream set of pitot tubes are at a location 100 feet (30.5 m) from the start of the channel.

3.3.3 Sharp Crested Weir

A sharp crested weir (see Figure 3.5) is located in the return channel approximately 30 ft (9.14 m) upstream of where the water enters the clarifier. The weir covers the whole width of the return channel and is five feet (152 cm) wide and two feet (61 cm) tall. It is equipped with a small rectangular opening that is one foot (30.5 cm) wide and eight inches (20 cm) tall, which is located in the lower middle portion and is used in order to release the water after testing is complete.

Figure 3.5 – Sharp Crested Weir

The construction of the weir is described in Hydraulic Effects of Safety End Treatments on Culvert Performance by Benson (2004); in this MS thesis the weir coefficient (C_d) was experimentally derived to be 0.618. With the weir coefficient known, it is then possible to calculate a flow rate based on the height of the water above the weir. This is accomplished according to Equation 3.1(King & Brater, 1963), where b is the width of the weir, g is the gravitational constant (32.2 ft/sec^2), h_w is the height of the water above the weir, and Q is the flow rate in ft^3/sec.

$$Q = C_d \frac{2}{3} b \sqrt{2g{h_w}^3} \tag{3.1}$$

To determine the height above the weir, a point gage (see Figure 3.6) was used that allowed measurements to be taken to the nearest thousandth of an inch. The gage was located approximately 16 ft (5m) upstream from the weir and was enclosed by a stilling well in order to reduce the effect of waves on the water surface. The gage was placed well upstream of the weir in order to take measurements where the surface profile is undisturbed. Normally, this upstream distance is approximately six times the maximum expected head (distance above the weir) (Mott, 2000). The stilling well was constructed

from clear piping that had an inside diameter of two inches (5 cm) and was open on both ends. The bottom of the stilling well was located approximately two inches (5 cm) from the bottom of the channel and the top was flush with the top of the channel. The gage is also equipped with a level bubble to ensure that readings were not affected by the angle of the gage.

In the MS thesis Hydraulic Performance of Bridge Rails based on Rating Curves and Submergence Effects by Brandon Klenzendorf (2007), the method for calibrating the point gage is discussed. According to Klenzendorf, several measurements were taken with the gage at the point when the water level was at the top of the weir, and the average value using the point gage for the top of the weir was found to be 0.954 ft (Klenzendorf, 2007). This value is then the effective zero point for the amount of head above the weir. In order to calculate the height above the weir, 0.954 ft was subtracted from the gage reading.

Figure 3.6 – Weir Point Gage

3.3.4 Pitot Tubes and Manometer Board

Nine pitot tubes connected to an inclined manometer board were utilized to measure the upstream and downstream water level height. Six tubes were used to measure the water depth upstream of the model and three were used to measure the downstream water depth. The pitot tubes were equally spaced across the width of the channel in groups of three and were located a sufficient distance away from the model so that the measurements would not be affected by turbulence or changes to the surface profile near the model. Figure 3.7 demonstrate the location of the pitot tubes in relation to the model.

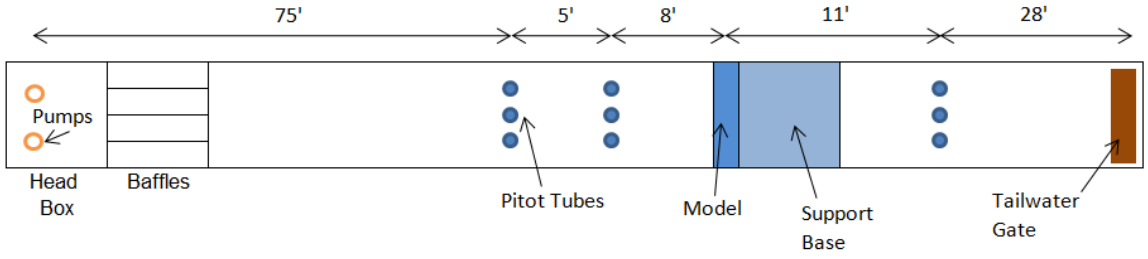

Figure 3.7 – Pitot Tube Locations (Diagram NTS)

The pitot tubes used are designed to measure static pressure head (water depth) and total pressure head (static head and velocity head). Two ports are located on the pitot tube for recording each of these heads, however, the port used for static pressure was the only one utilized in this research. A schematic of the pitot tubes that were used is shown below in Figure 3.8.

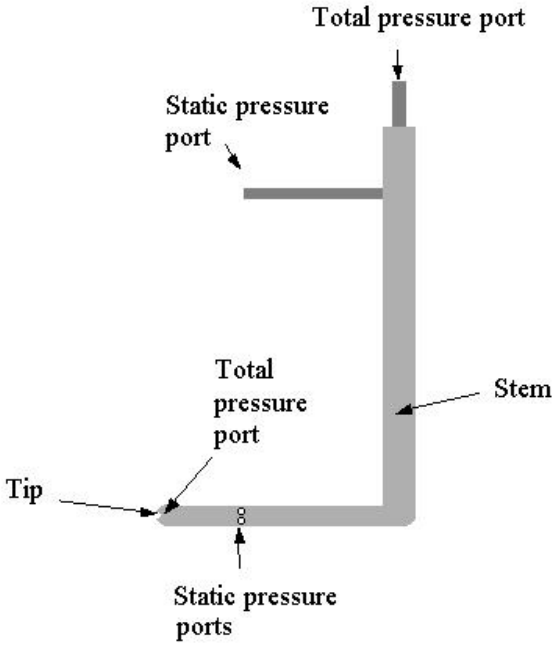

Figure 3.8 – Pitot Tube Schematic

The pitot tubes were then connected to an inclined manometer (see Figure 3.9) board by flexible plastic tubing attached to the static pressure port. An inclined manometer is used in leiu of a vertical one, because of the increased precision that is achieved. This increase in precision is due to the fact that a small vertical change will result in a large change along the incline. The construction of the manometer board and its calibration are described by Brandon Klenzendorf (2007).

Figure 3.9 – Inclined Manometer Board

The manometer board consisted of nine rigid plastic tubes connected on the bottom end to the pitot tubes (via the flexible tubing) and on the upper end to a manifold (via flexible tubing). The manifold was used to flush water through the system in order to remove any air in the lines prior to testing. Also, small holes were drilled into the top of the rigid pipes so that the water in the tubes would be exposed to atmospheric pressure. Since the water in the manometer board and water flowing in the channel are both exposed to atmospheric pressure, the water level in both should be the same.

To gauge the height of water in the channel with the inclined manometer board two pieces of information must be known, which are: the angle of the manometer board and the height of the zero measurement (on the manometer board) above the channel bottom. The angle of inclination of the manometer board used for this research is approximately 25.5° (Klenzendorf, 2007). Therefore, a vertical height can be calculated simply by multiplying the inclined reading by the sine of the angle of inclination. Equation 3.2 is included below to better illustrate how this is accomplished, where h_v is

the vertical height, h_i is the height recorded on the incline, and θ is the angle of inclination.

$$h_v = h_i \sin\theta \tag{3.2}$$

In order to determine the height of the water above the channel bottom, however, the height of the zero measurement must also be known. Surveying equipment was used to accurately measure this distance, (Klenzendorf, 2007). It was determined that the elevation difference between the channel and the zero measurement is approximately equal to 0.835ft (25.5 cm). Therefore, to determine the height of the water above the channel bottom this difference must be added to the vertical height calculated in Equation 3.2. This is further illustrated below by Equation 3.3. In this equation, H is the height of the water above the channel, h_v is the vertical height calculated from the inclined manometer board measurement, and h_{mb} is the height of the manometer board zero reading, which is the height of the water above the channel bottom when the manometer board registers a zero value.

$$H(ft) = h_v + h_{mb} = h_i sin(25.5^0) + 0.835 \tag{3.3}$$

3.3.5 Tailwater Gate

A gate that is hinged at the top and connected at the bottom with steel cables was installed prior to the main channel discharge into the return channel. The steel cables are connected to a crank that control the height of the gate, which then allows for testing the effects of submergence downstream of the model. This is accomplished by lowering the gate into the water and creating an obstruction that produces a hydraulic jump. The hydraulic jump is the result of the specific energy of the water changing from

supercritical to subcritical flow. When this happens the water depth increases, which allows for testing the affects of downstream submergence on the upstream water depth. As the gate is lowered, the obstruction becomes greater and the downstream water depth increases. This affects the upstream water depth by impeding the flow through the orifice, which then causes the upstream water depth to increase.

Figure 3.10 – Tailwater Gate

3.4 METHODOLOGY

As with any experiment, specific methods must be followed to ensure the reliability and accuracy of the data being gathered. This section will discuss the start up procedure, rating curve data gathering and submergence testing data gathering procedures, and shut-down procedures.

3.4.1 Start-up Procedure

This sub-section will discuss the start-up procedure for both the rating curve and submergence tests. To begin testing, the removable boards were inserted in the model base, and the small rectangular opening in the sharp crested weir was closed. The next step was to make sure that the pitot tubes were working properly. This was done by connecting the manifold on the manometer board to a water faucet located on the exterior of Building 120, which was located next to the channel. With the manifold connected to the water line, the water was then turned on and water allowed to flow into the manometer board and out to the pitot tubes. At this point the flexible tubing connecting the pitot tubes and manometer board and the rigid tubes of the manometer board were both monitored for the presence of air bubbles. Also, the pitot tube's static ports were checked to determine if there was any blockage. The pitot tubes used were equipped with eight ports. If any of the ports were clogged, they were either unclogged via a wire brush or were replaced with a new pitot tube. After the tubes were shown to be in working order and the air in the lines was flushed, the valves on the pumps were then adjusted and the pumps turned on. The water to the manifold was then turned off after the pitot tubes were submerged. This ensured that air would not be allowed to re-enter the lines. The last step was to allow the pumps to run for a minimum of 45 minutes before data was collected. This time was determined during previous research by Klenzendorf (2007), and was set so that enough time was allowed for water to fill up the return channels and steady state conditions could be achieved before flow measurements at the sharp crested weir were recorded.

3.4.2 Rating Curve Testing Procedure

During the development of the rating curves for the TCTBs only the six upstream pitot tubes were used. Three tests were conducted for each flow rate, with a minimum of two minutes between each test. Each test consisted of recording the height readings on the manometer board for each of the pitot tubes, and recording the measurement taken from the point gage for calculating the flow. The precision of the manometer board readings is 0.005 ft and was taken from the bottom of the meniscus. The point gage's precision is 0.001 ft and was recorded when the tip was observed to make contact with the water surface. Due to slight oscillations in the water's surface the arithmetic mean of the values recorded in the three tests are used in the development of the rating curve.

When testing was accomplished for multiple flow rates on the same day, the valves and pump combinations could be changed after one test was complete. Since water had already filled the return channels, 30 minutes was allowed for the flow to stabilize and reach steady state conditions, instead of the 45 minutes that was required for start-up.

3.4.3 Submerged Testing Procedure

For testing the affect of submergence on the water height upstream, all nine pitot tubes were utilized. Six pitot tubes were located upstream of the model and were used to measure the upstream water depth. Three additional pitot tubes were located downstream of the model and were used to measure downstream water depth. During submergence testing six tests were performed for each different position of the tailwater gate. Six tests were performed instead of three, because of the turbulence generate by the hydraulic jump. At lower downstream water elevations, as much as one and a half inches of change

was detected during a test, but as the water level increased the readings became much more stable. However, for the sake of consistency, six tests were performed for all the different tailwater gate positions.

The first test was conducted when the tailwater gate produced a hydraulic jump that brought the downstream water elevation to the top of the model support base. At this point the downstream water depth should have little effect on the upstream water depth and is an appropriate starting point for testing. Also, at this point, the pitot tubes become submerged and the water to the manifold on the manometer board is shut off, so as to prevent any air from entering the lines. As with the rating curve tests, two minutes is allowed in-between each of the tests, in order to detect any fluctuations that might be occurring. A minimum of eight tests were performed at the same flow rate and different tailwater gate positions, and four such series of tests were performed at different flow rates.

Unlike the rating curve tests, the flow rate was not changed between tests. Since the flow rate did not change, the only part of the experiment that required time to stabilize was the downstream water depth. A minimum of 15 minutes was allowed for the water level to stabilize after one test was complete and a new tailwater gate position established. Also, as it was with setting the tailwater gate so that the downstream water level was at the height of the model base, some adjustment was necessary between tests in order to perform experiments where the water elevation was not too similar to the last experiment and did not deviate too much as to create too large a gap between experiments.

3.4.4 Shut-down Procedure

The shut-down procedure for both the rating curve and submergence tests is the same. The pumps are first shut off and some of the water is allowed to drain. At this time, the tailwater gate is also raised (if performing submergence test). Once the water level in the main channel has dropped it is then possible to remove the boards on the side of the model base and open the gate on the sharp crested weir, so that the remaining water can drain back to the reservoir.

Chapter Four

Model Derivation

4.1 INTRODUCTION

The purpose of this research is the development of a rating curve that will describe the relationship between upstream water energy and flow for Temporary Concrete Traffic Barriers (TCTB). To do this, two different models need to be developed. The first model, the Rating Curve Model is a model that develops the link between upstream energy and flow, without the presence of a downstream obstruction. This model will demonstrate the ideal condition, where water flowing through the orifice and over the top of the barrier is not affected by backwater. The second model, the Submergence Model, will then describe the effects of an impediment downstream that forces water to back up on the downstream side of the TCTB. This water will then reduce flow through the orifice in the barrier and cause the potential energy (water height) upstream of the barrier to increase.

4.2 RATING CURVE MODEL

This research builds upon a previous study conducted by Charbeneau et al. (2006). In the development of the rating curve model, the first step was to assess the different flow types that would be occurring as water passes from one side of the TCTB to the other. For TCTBs there are three possible flow regimes: Type 1 flow is a weir type flow in which water flows through the scupper drain but is not completely submerged, Type 2 flow is an orifice type flow, where the water level upstream of the barrier is above

the height of the drain, and Type 3 flow occurs when water overtops the barrier and is a combination of orifice and weir flow. The equations governing each flow type are provided below in Equations 4.1, 4.2, and 4.3. In these equations energy (e), expressed in units of length, is used. In order to determine the energy upstream of the barrier (e_u), the water elevation (potential energy) and flow rate is used to calculate the kinetic energy. With the kinetic energy calculated, this number can simply be added to the potential energy that is already being measured in order to determine the total energy upstream. Furthermore, in these equations Q represents the flow rate, g is the gravitational constant, A_r, is the area of the barrier, C_b C_c and C_d are experimentally derived coefficients, F_o is the fraction of open space in the barrier, and all other terms are detailed in the following paragraph.

Type 1 $$\frac{Q}{A_r\sqrt{gh_r}} = C_b F_o \frac{h_r}{h_{rL}}\left(\frac{2e_u}{3h_r}\right)^{1.5} \quad (4.1)$$

Type 2 $$\frac{Q}{A_r\sqrt{gh_r}} = C_b C_C F_o \sqrt{2\left(\frac{e_u}{h_r} - C_c\frac{h_{rL}}{h_r}\right)} \quad (4.2)$$

Type 3 $$\frac{Q}{A_r\sqrt{gh_r}} = C_b C_C F_o \sqrt{2\left(\frac{e_u}{h_r} - C_c\frac{h_{rL}}{h_r}\right)} + C_d\left(\frac{2}{3}\right)^{1.5}\left(\frac{e_u}{h_r} - 1\right)^{1.5} \quad (4.3)$$

Figure 4.1 illustrates the different flow types, which are defined by the water height. Also, in this figure, several key parameters used in the creation of the model are shown. The first parameter of interest is the term H_u, which is the overall height of the water that is measured by the pitot tubes at a location upstream of the barrier. Next, h_b is defined as the height of the support base, which is discussed in Section 3.2.3. Furthermore, h_u is the difference between H_u and h_b, i.e. $h_u=H_u-h_b$. Furthermore, h_r is the

height of the barrier, and h_{rl} is the height of the drain opening. Lastly, b is the width of the channel, and b_p is the support base with, which is the difference between b and b_{rl}, (b_p=b-b_{rl}), where b_{rl} is the width of the drainage opening. These terms describe the physical properties of the barrier being tested and are important in deriving the equations for the different flow types in the subsequent sections.

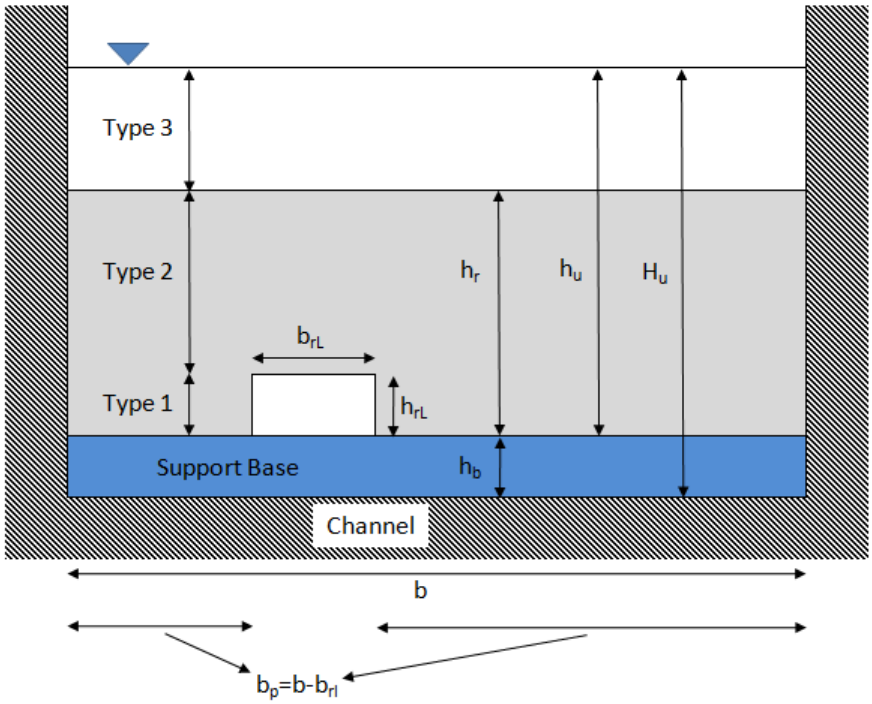

Figure 4.1 – Flow Type Schematic for MSSCB (NTS)

4.2.1 Type 1 Flow

In Type 1 flow, water is allowed to pass through the scupper drain , but the water level is less than the height of the drain opening. For this flow regime, water is forced to go from a subcritical flow upstream of the barrier, to a critical flow at the barrier, and

then to supercritical as the water flows through the opening. This is because the barrier acts as an obstruction to the flow, which causes the potential energy to increase and the kinetic energy to decrease upstream of the barrier. Downstream of the barrier, the water is then in a supercritical state, because of the lack of an obstruction. Therefore, it can be surmised that at the barrier, critical flow will be developed. This is extremely helpful information, and serves as the launching point for deriving the mathematical model developed by Charbeneau et al (2006). It is also important to know that, as it was discussed in Section 2.3, the height of the water upstream of the barrier can be related to the critical height by Equation 2.8, or $h_c=2h_u/3$, because the critical height cannot be measured, while the height upstream is readily measurable.

With the critical height related to upstream water depth, it is also helpful to know that at critical flow the Froude number is equal to a value of one. This is because the Froude number is the ratio between inertial forces and gravitational forces, or the ratio between supercritical flow and subcritical flow. Equation 4.4 below, describes this relationship, where v is the velocity, g is the gravitational constant, and D is a characteristic length (water depth).

$$Fr = \frac{\mathrm{v}}{\sqrt{gD}} \tag{4.4}$$

If the Froude number is then set to one, and Equation 4.4 solved for the velocity term, the results is then presented below in Equation 4.5, where h_c is the critical height.

$$v_c = \sqrt{\mathrm{gh_c}} \tag{4.5}$$

This is very helpful, because we now can determine the velocity through the drain opening, which is a function of gravitational forces and the water height upstream, by substituting Equation 2.8 into Equation 4.5 to obtain the following result, Equation 4.6.

$$v_c = \sqrt{g\left(\frac{2}{3}h_u\right)} \tag{4.6}$$

The flow rate through the scupper drain can then be calculated through the use of the continuity equation, Q = vA, where v is the velocity and A is the area of flow. According to Charbeneau et al (date), the area of flow through a drain is diminished by horizontal contractions that occur as water flows through the opening. To account for the reduction in area, coefficient values can be experimentally determined that account for these losses. Figure 4.2, below, illustrates this phenomenon, where the water entering the drain is contracted. The coefficient C_b is used here to describe the decrease in the effective area by which the water is flowing through the opening. This figure shows the flow being forced to the middle as water passes through the orifice, which then causes a decrease in the effective width as can be seen in Figure 4.3.

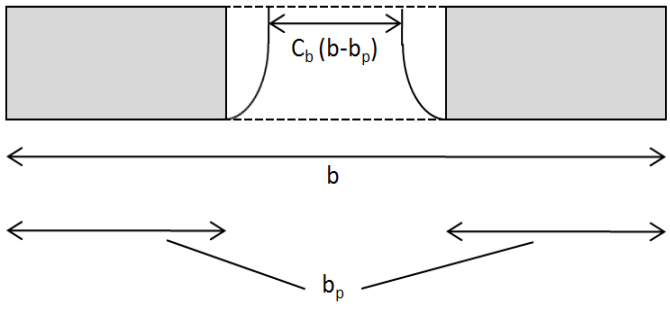

Figure 4.2 – Plan View of Type 1 Flow

Figure 4.3 – Type 1 Flow

What we are left with then is Equation 4.7, which describes the flow rate at the location of critical depth (at the barrier) based on the assumptions described above.

$$Q = Av_c = C_b(b - b_p)\left(\frac{2}{3}h_u\right)\sqrt{g\left(\frac{2}{3}h_u\right)} \tag{4.7}$$

The next step is then to write the equation in a form that will easily allow the comparison of different barriers, and derive it in a way such that it is non-dimensional. Non-dimensionalizing the equation transforms the flow to a per unit basis, so that the equation will be applicable to any length of barrier, and rearranging the terms so that the flow area is based on a fraction of open space facilitates easy comparison between barriers based on the amount of area is allocated to drainage. The fraction of open space

is then given below by Equation 4.8, where A_o is the cross-sectional area of the drain perpendicular to the flow and A_r is the cross-sectional area of the barrier perpendicular to the flow, which includes the drain area, and all other terms have been defined previously.

$$F_o = \frac{A_o}{A_r} = \frac{(b-b_p)h_{rL}}{bh_r} \tag{4.8}$$

Next, by taking Equation 4.7 with 4.8 and employing some algebra, Equation 4.9 can be derived, which is the non-dimensional equation for Type 1 flow.

$$\frac{Q}{A_r\sqrt{gh_r}} = C_b F_o \frac{h_r}{h_{rL}}\left(\frac{2h_u}{3h_r}\right)^{1.5} \tag{4.9}$$

4.2.2 Type 2 Flow

Type 2 flow occurs when the water level rises above the height of the drainage opening, and is modeled as an orifice flow according to Charbeneau et al. (2006). This flow regime, like Type 1 flow, is also affected by contractions at the opening. Figure 4.4 below, shows the vertical contraction that occurs during orifice flow. For orifice flow both the vertical and horizontal contractions must be considered in calculating the area of flow.

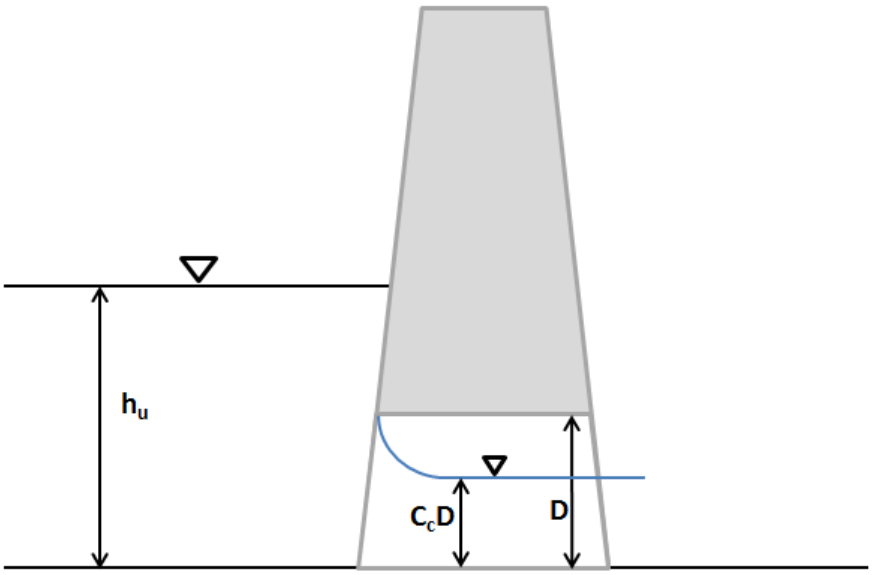

Figure 4.4 –Profile View of Type 2 Flow

The first step in developing the equation is realizing that the energy upstream of the barrier and at the barrier will be the same (given the assumptions made in Section 2.2). Additionally, like it was with Type 1 flow, it can be assumed that the flow upstream will be subcritical, due to the obstruction of the barrier. This assumption leads to the simplification of the energy equation, because the upstream water velocity (kinetic energy) will negligible when compared to the water depth (potential energy), i.e. $\frac{v_u}{2g} \ll h_u$. Next, it should also be noted that the water depth (potential energy) at the barrier will be related to the height of the drain opening multiplied by the coefficient Cc, as described in Section 4.1.1, because of the contraction that occurs when water flows through the orifice. Finally, it is possible to develop the energy equation, Equation 4.10. In this equation the subscript u refers to the upstream position, the subscript m refers to a location at the model, and all other terms have been defined previously.

$$h_u = C_c h_{rL} + \frac{v_m{}^2}{2g} \tag{4.10}$$

The next step is then to use the continuity equation (Q=Av) as we did in evaluating Type 1 flow. By rearranging Equation 4.10 we can solve for v_m. This will give the velocity portion of the continuity equation and is given below as Equation 4.11.

$$v_m = \sqrt{2g(h_u - C_c h_{rL})} \tag{4.11}$$

The area can then be realized as the height of the barrier orifice multiplied by the coefficient C_c times the width of the barrier orifice multiplied by the coefficient C_b. Plugging the values for area and velocity into the continuity equation we are then left with Equation 4.12.

$$Q = Av_m = C_b(b - b_p)C_c h_{rL}\sqrt{2g(h_u - C_c h_{rL})} \tag{4.12}$$

However, as it was done for Type 1 flow, we must also convert the equation to the non-dimensional form. The result of the algebraic conversion is then given by Equation 4.13.

$$\frac{Q}{A_r\sqrt{g h_r}} = C_b C_C F_o \sqrt{2\left(\frac{h_u}{h_r} - C_c \frac{h_{rL}}{h_r}\right)} \tag{4.13}$$

The last step is then to determine the height upstream which will be the transition point between Type 1 and Type 2 flow. To do this we can set the equations for each of the flow types equal to each other. The result is a cubic equation in terms of the upstream water depth, in which there are three roots. The first root is equal to a value of -3 (which has no physical meaning), and the second two roots equals 3/2. The resultant equation with respect to upstream water depth is then given by Equation 4.14.

$$\frac{h_u}{\mathrm{h_r}} = \frac{3}{2}\mathrm{C_c}\frac{\mathrm{h_{rL}}}{\mathrm{h_r}} \tag{4.14}$$

This equation is non-dimensional with respect to the height of the barrier, as are the equations for Type 1 and 2 flows. Also, it should be noted that this equation is equivalent to Equation 2.8, which was derived earlier in this paper in Section 2.3. It is at this point that the Type 1 and 2 flow curves intersect and the derivatives of the curves are equal, which creates a smooth transition point between the two flow types.

4.2.3 Type 3 Flow

Type 3 flow can be explained through the superposition of orifice and weir flow, in which the orifice flow is described by the equation for Type 2 flow and weir flow is that of a broad crested weir. The equation for broad crested weir flow is then given by Equation 4.15 (Bos, 1989). This equation is similar to Equation 3.1 used for calculating the flow rate in the experimental setup, however, the difference being that the weir used in that situation is a sharp crested weir. Also, in this equation an extra term is added, C_v, which accounts for a loss in the velocity head as the water passes over the weir.

$$Q = C_d \mathrm{C_v}\frac{2}{3}b\sqrt{\frac{2}{3}g{h_w}^3} \tag{4.15}$$

If this equation is then converted into the non-dimensional form, as the equations for Type 1 and Type 2 flows were, the result is Equation 4.16. In this equation, it should be noted that the term C_v is omitted because combining it with C_d will result in a single coefficient, which is more practical for modeling purposes. Also, the term h_w is

equivalent to the height of the water above the weir, which is the difference between the water height upstream and the barrier height (h_w=h_u-h_r).

$$\frac{Q}{A_r\sqrt{gh_r}} = C_d\left(\frac{2}{3}\right)^{1.5}\left(\frac{\mathrm{h_u}}{\mathrm{h_r}} - 1\right)^{1.5} \tag{4.16}$$

By combine Equations 4.13 and 4.16, we are then left with a non-dimensional equation for modeling Type 3 flow (Equation 4.17).

$$\frac{Q}{A_r\sqrt{gh_r}} = \mathrm{C_b C_C F_o}\sqrt{2\left(\frac{\mathrm{h_u}}{\mathrm{h_r}} - \mathrm{C_c}\frac{\mathrm{h_{rL}}}{\mathrm{h_r}}\right)} + C_d\left(\frac{2}{3}\right)^{1.5}\left(\frac{\mathrm{h_u}}{\mathrm{h_r}} - 1\right)^{1.5} \tag{4.17}$$

4.3 SUBMERGENCE MODEL

The Submergence Model describes the effects of an obstruction that forces water to back up on the downstream side of the TCTB. This water will then hinder flow through the barrier and cause the potential energy (water height) upstream to increase. The increase in the water height will then be a departure from the prediction given in the rating curve model. To describe this departure two methods have been developed. The first is a model developed by Villemonte (1947), which is based on the general weir equation and the principle of superposition. This model, however, tends to overestimate the effects due to low flow rates and underestimate those due to high flow rates (Klenzendorf, 2007). The second is an empirically derived equation developed from the Villemonte model, which is described by Klenzendorf (2007). In this model, the non-dimensional flow rate is included in the equation in order to represent the impact that changing the flow will have on the rating curve.

4.3.1 Villemonte Model

As previously noted, the Villemonte Model describes the effect that an increase in downstream water depth (submergence) imparts to upstream water depth. To describe the interaction between upstream and downstream water depth the principle of superposition was used, where the net flow rate (Q) is a function of the upstream and downstream discharges Q_1 and Q_2 that would occur under conditions without submergence.

Figure 4.5 – Villemonte Model (Villemonte, 1947)

The resulting statement is then given below by Equation 4.18, where the net flow is equal to the difference between flow upstream and downstream ($Q = Q_1 - Q_2$) ,and the equation has been algebraically transformed so that the left hand side represents a submergence coefficient.

$$\frac{Q}{Q_1} = 1 - \frac{Q_2}{Q_1} \tag{4.18}$$

This equation, however, proved to be invalid when compared to the data Villemonte conducted on various weirs. Nevertheless, a relationship was discovered between Equation 4.18 and the data, when a multiplicative and an exponential constant (k,m) were added to the right side of the equation. The result of these additions leads to Equation 4.19, given below, which is the general form of the submergence model.

$$\frac{Q}{Q_1} = \mathrm{k}\left(1 - \frac{\mathrm{Q_2}}{\mathrm{Q_1}}\right)^{\mathrm{m}} \tag{4.19}$$

If we then insert the general form of the weir equation (Equation 2.9) into Equation 4.19 the result is given by Equation 4.20, in which the exponent n is dependent on the particular weir being used.

$$\frac{Q}{Q_1} = \mathrm{k}\left(1 - \frac{\mathrm{Cbh_2}^{\mathrm{n}}}{\mathrm{Cbh_1}^{\mathrm{n}}}\right)^{\mathrm{m}} \tag{4.20}$$

Furthermore, C and b can be removed from the expression because they are a constant for both the upstream and downstream flows, and the coefficient *k* can be removed, because it was experimentally determined to have a value of 1 for weirs with horizontal crests by Villemonte. This results in Equation 4.21. In this equation energy (e), expressed in ft, has been substituted for the height above the weir, where the head datum is measured from the support base instead of from the top of the weir, as was done in the Villemonte model. Also, because the LPCB has a horizontal crest, a value of 1.5 can be inserted for n.

$$\frac{Q}{Q_1} = \left(1 - \left(\frac{\mathrm{e_d}}{\mathrm{e_u}}\right)^{1.5}\right)^{\mathrm{m}} \tag{4.21}$$

However, since the LPCB includes orifice flow, the value of 1.5 for n may not be entirely correct. It should be noted though, that this equation is still used, because it has been found to produce reasonable results.

4.3.2 Empirical Model

Another model has been developed by which the Villemonte model is adapted to account for changes in the flow rate. In this model proposed by Klenzendorf (2007), the non-dimensional flow rate is included in the power term, and an additional parameter (A) is inserted into the equation to create a lower bound, where the downstream water height has a limited effect on the upstream water elevation. Also, the power term n is assumed to be one. This is because the value of 1.5 used in the Villemonte model is derived from the weir equation, and the addition of orifice flow will alter this term. The result of these changes is given below in Equation 4.22, where F_Q is the non-dimensional flow rate, B is the model coefficient, and all other terms have been defined previously.

$$\frac{Q}{Q_1} = \left(\frac{\Delta e}{Ae_u}\right)^{1/BF_Q} \tag{4.22}$$

Furthermore, the value of A used in this report is taken from an experiment by Klenzendorf. To find a suitable value for A, the type T203 bridge rail submergence test data was compared to Equation 4.22. When different values for A were plugged into the equation a plot of the standard error versus A was developed. This graph is presented in Figure 4.6. In this graph, there appears to be a local minimum when A equals 2/3. Since the flow through the bridge rail is similar to that of a traffic barrier, this value is used as the fitting parameter in this research.

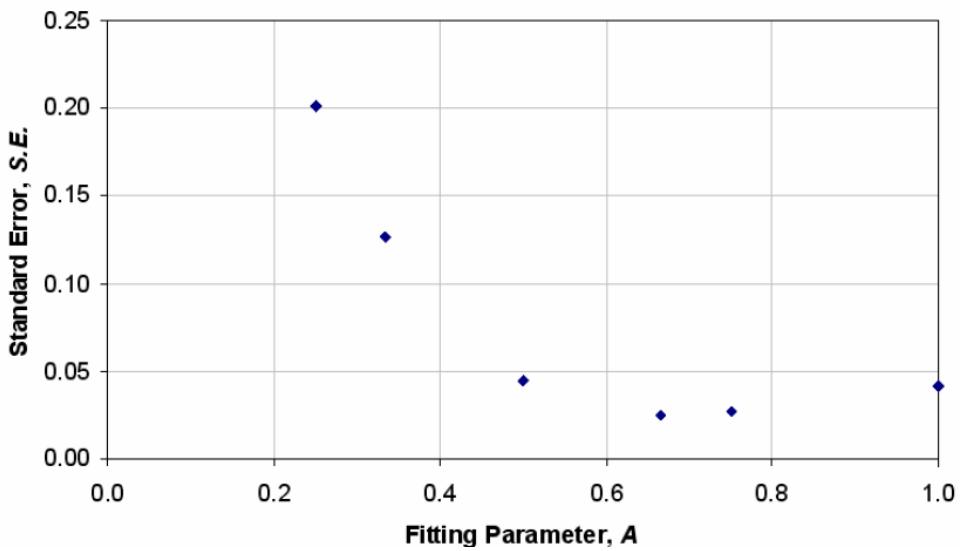

Figure 4.6 – Fitting Parameter A (Klenzendorf, 2007)

Chapter 5

Experimental Results

5.1 INTRODUCTION

The purpose of this research is the development of a hydraulic rating curve that describes the relationship between energy upstream of a TCTB to differing flow rates. The following sections will discuss the rating curves that were developed for both the submerged and unsubmerged conditions using the model equations discussed in Chapter 4 with experimental data collected at the University of Texas J.J Pickle Research Campus.

5.2 RATING CURVE DATA

Figures 5.1 through 5.3 summarize the data gathered as prescribed in Section 3.4, where the ordinate values are expressed in units of feet and the abscissa is the flow rate. These graphs alone, however, do not constitute a model, as was developed in Chapter 4 of this report. Furthermore, only three sets of data are given below, because the data for the MSSCB was used in the analysis of both the SSCB and SSCBSPL.

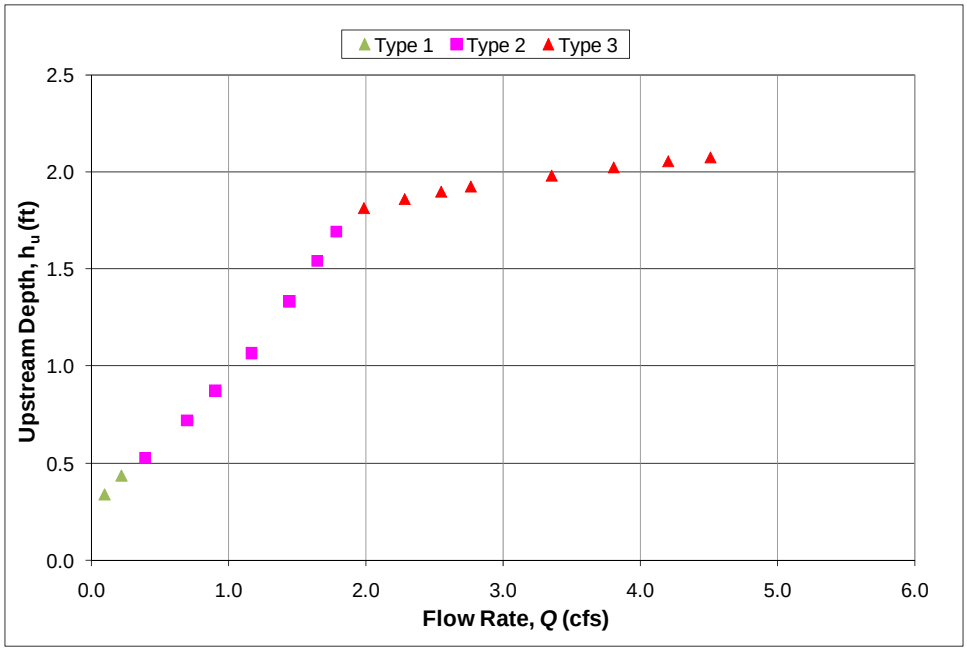

Figure 5.1 – MSSCB Rating Curve Data

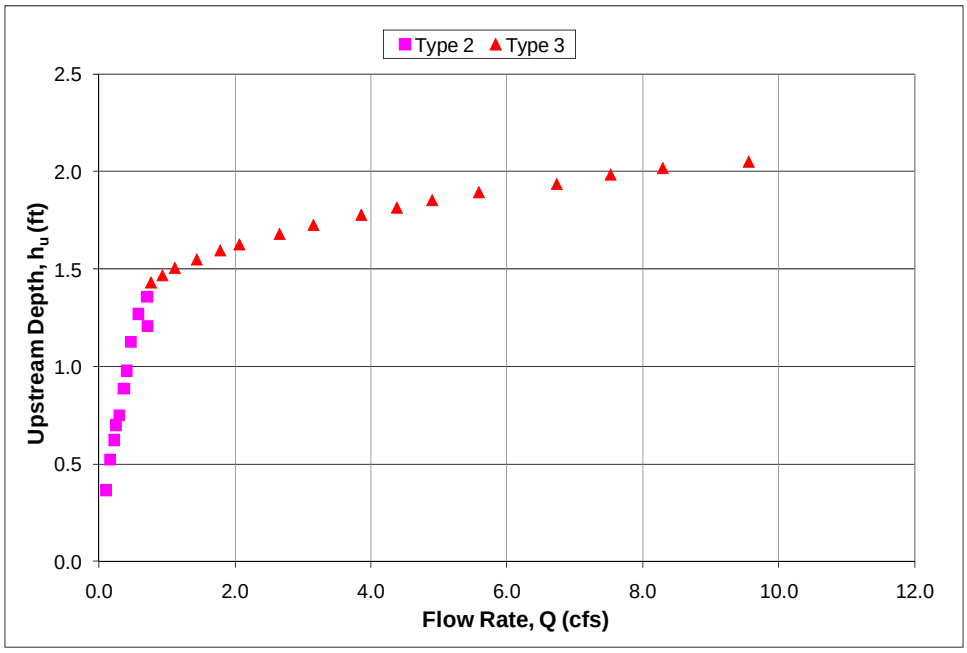

Figure 5.2 – CSB Rating Curve Data

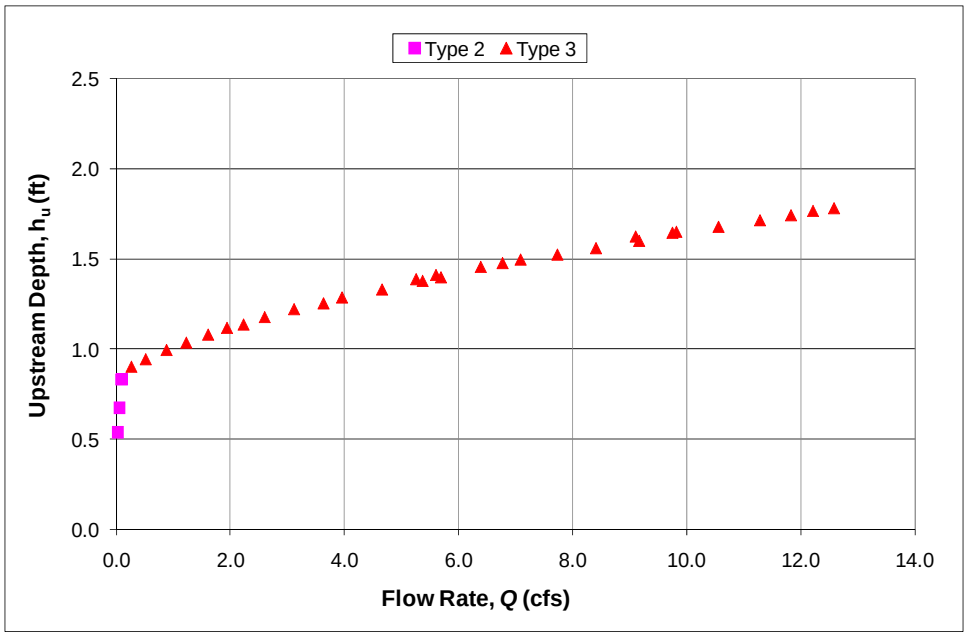

Figure 5.3 – LPCB Rating Curve Data

In order to obtain a graph which represents the model equations and the data in Figures 5.1-5.3, the Excel Macro Tool was utilized to create a function that can be used in an Excel spreadsheet. This function, Qnon, calculates the non-dimensional flow rate based on the input variables e (e_u/h_r), fo (fraction of open space), a (h_{rl}/h_r), and the coefficient values C_b, C_c, and C_d.

```
Function Qnon(e, fo, a, cb, cc, cd)
  If (e < 1.5 * cc * a) Then
    Qnon = cb * fo * (1 / a) * (2 * e / 3) ^ 1.5 'Type 1 Flow'
  Else
    Qnon = cb * cc * fo * Sqr(2 * (e - cc * a)) 'Type 2 Flow'
  End If
    If e > 1 Then
    Qnon = Qnon + cd * (2 / 3 * (e - 1)) ^ 1.5 'Type 3 Flow'
  End If
  End Function
```

Microsoft Excel Solver and regression was then utilized to fit the model to the data by changing the coefficient values of C_b, C_c, and C_d, where the coefficient values were subject to the following constraints:

$$0.0 < C_b \leq 1.0 \quad (5.1)$$

$$0.0 < C_c \leq 1.0 \quad (5.2)$$

$$0.0 < C_d \quad (5.3)$$

The constraints are necessary because in the developed equations, C_b and C_c describe the contraction that happens when water passes through the orifice, and a zero value would result in no flow in the horizontal or vertical directions respectively. C_d, on the other hand, has to be greater than zero, because a negative value would produce negative flow after the water overtopped the barrier and a value of zero would result in zero flow over the barrier. The results of this analysis are given below in Figures 5.4-5.6, where the abscissa and ordinate are in the non-dimensional form that is given in the model equations developed by Charbeneau et al. (2008). Also, the coefficients that were calculated for each of the barriers are given below in Table 5.1 with the associated standard error between the rating curve and the observed data.

Table 5.1 – Rating Curve Coefficient Values

	MSSCB	CSB	LPCB
Cb	0.588	0.477	0.177
Cc	1.000	0.855	0.338
Cd	0.843	1.011	0.900
S.E.	3.20%	8.64%	4.41%

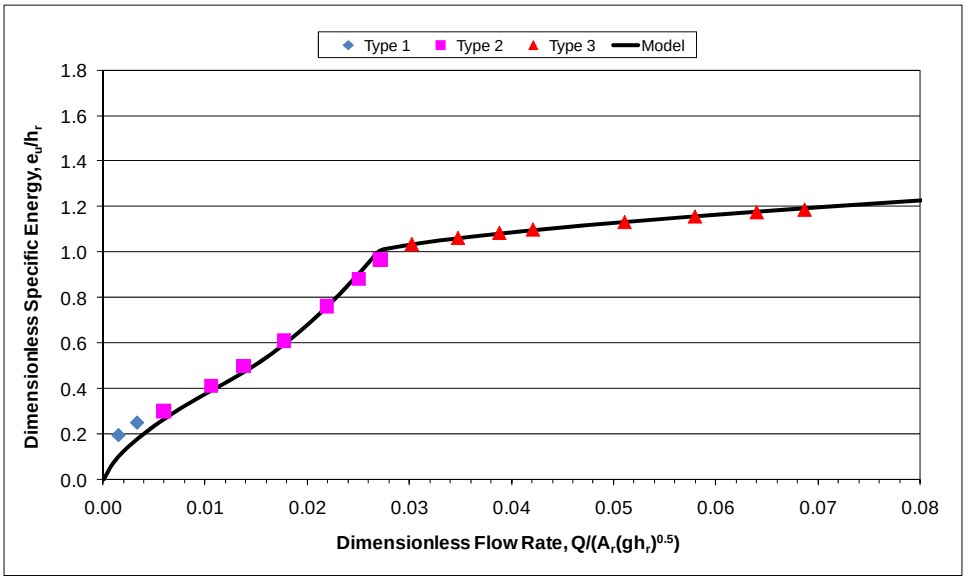

Figure 5.4 – MSSCB Rating Curve

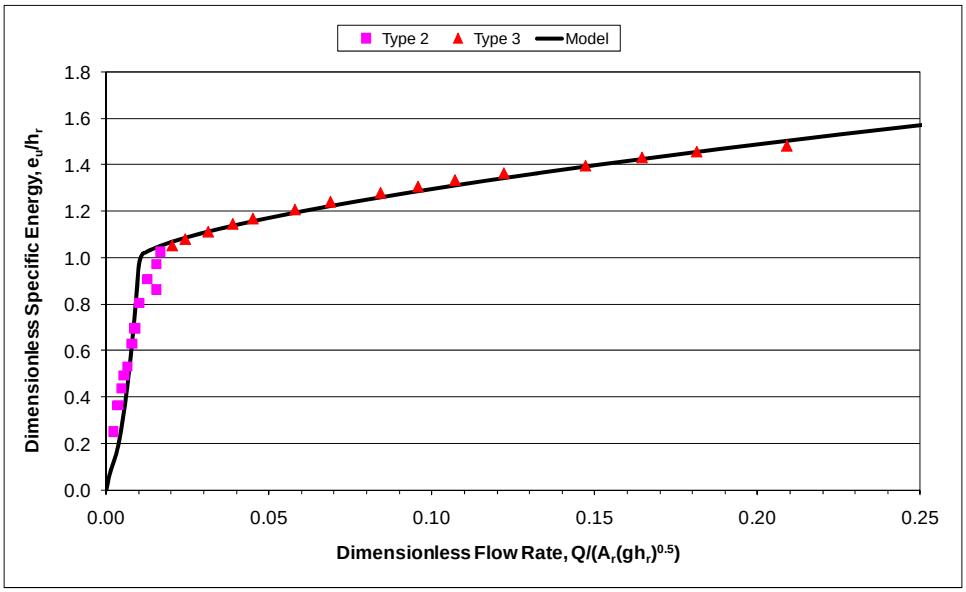

Figure 5.5 – CSB Rating Curve

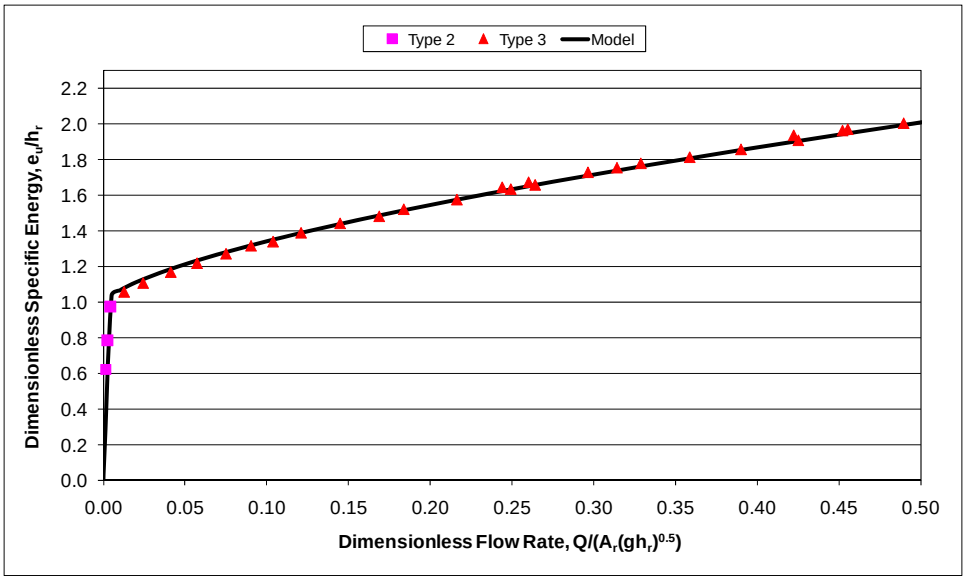

Figure 5.6 – LPCB Rating Curve

Furthermore, in order to understand the effects on the actual barrier, we can transform the model output through simple algebra, to get the flow rate and energy upstream. For example, using the function Qnon it is possible to solve for the non-dimensional flow, given the non-dimensional specific energy. If the non-dimensional values are multiplied by the physical parameters of the barrier, the actual flow rate and upstream energy can be calculated. This is shown below by Equation 5.4 and 5.5.

$$Q = \frac{Q}{A_r\sqrt{gh_r}} \times A_r\sqrt{gh_r} = \frac{Q}{A_r\sqrt{gh_r}} \times b_r\sqrt{gh_r^3} \tag{5.4}$$

$$e_u = \frac{e_u}{h_r} \times h_r \tag{5.5}$$

Moreover, if the LPCB is analyzed, it is possible to develop a graph similar to Figure 5.7, where the flow is based on a per linear foot of barrier basis (b_r=1).

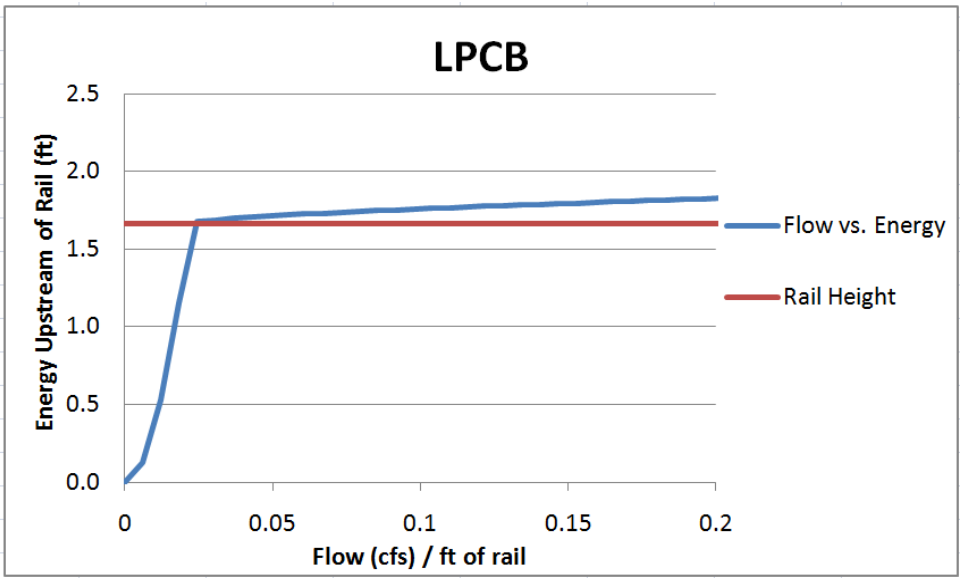

Figure 5.7 – LPCB Example Rating Curve

5.3 SUBMERGENCE DATA

The data presented below in Figures 5.8-5.10 are the result of testing conducted according to Section 3.4.3. A diagonal line with slope 1.0 has been inserted on the graphs to visualize when an incremental increase in downstream depth will result in the same increase in upstream height. This line is considered the asymptote of the data, because when the data approaches this line the barrier's effect is negligible and the data will continue to increase and follow this line. Also, it should be noted that the flow rate in the legend is given as the range of values that were recorded during a test. This is because the flow varied slightly during testing.

Testing was conducted at four different flow rates in order to determine the effect that flow will have on the submergence ratio. In the first model, there will be no effect due to varying the flow, because the Villemonte Model is independent of flow; however,

the Empirical model is implicit with respect to flow and a series of curves will be developed to describe the effect of submergence for different values of Q.

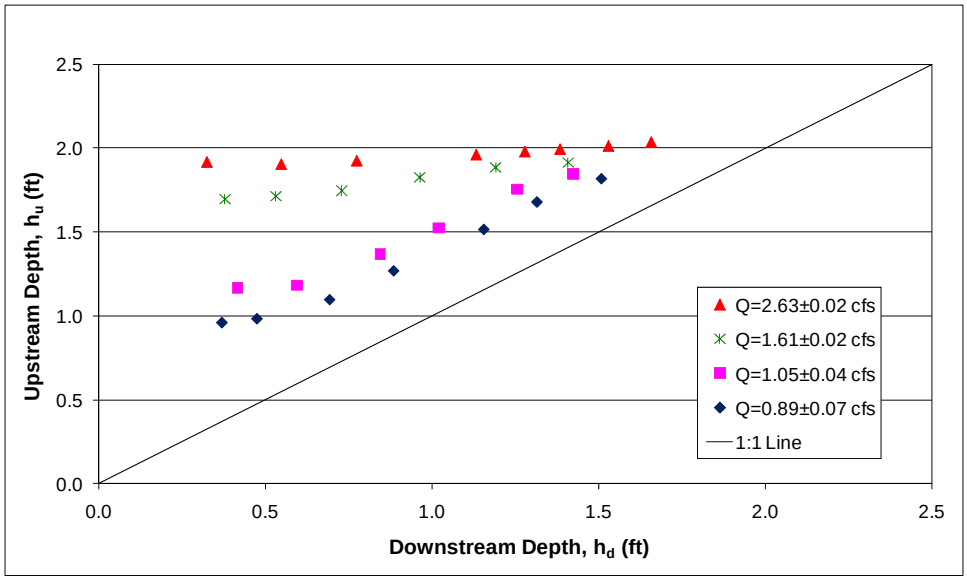

Figure 5.8 – MSSCB Submergence Data

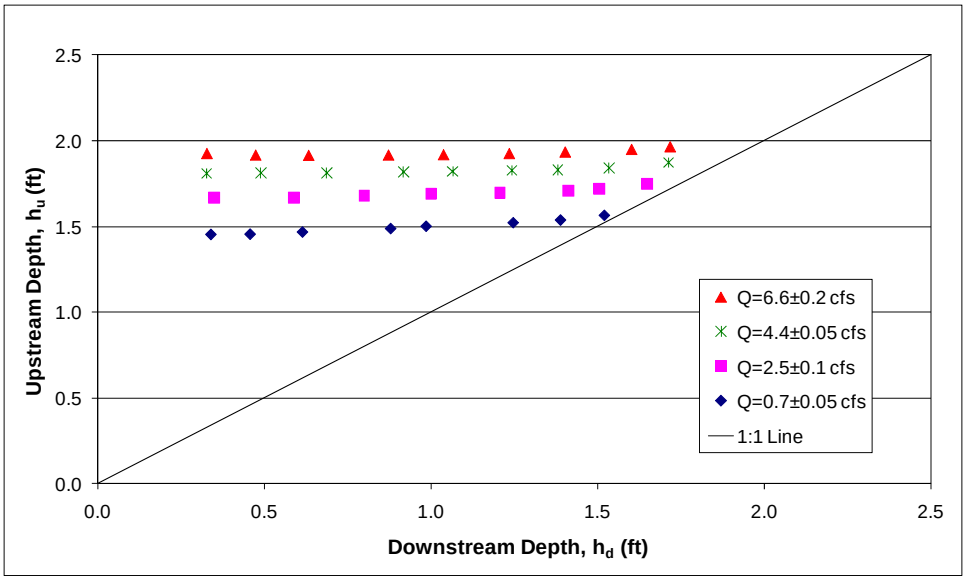

Figure 5.9 – CSB Submergence Data

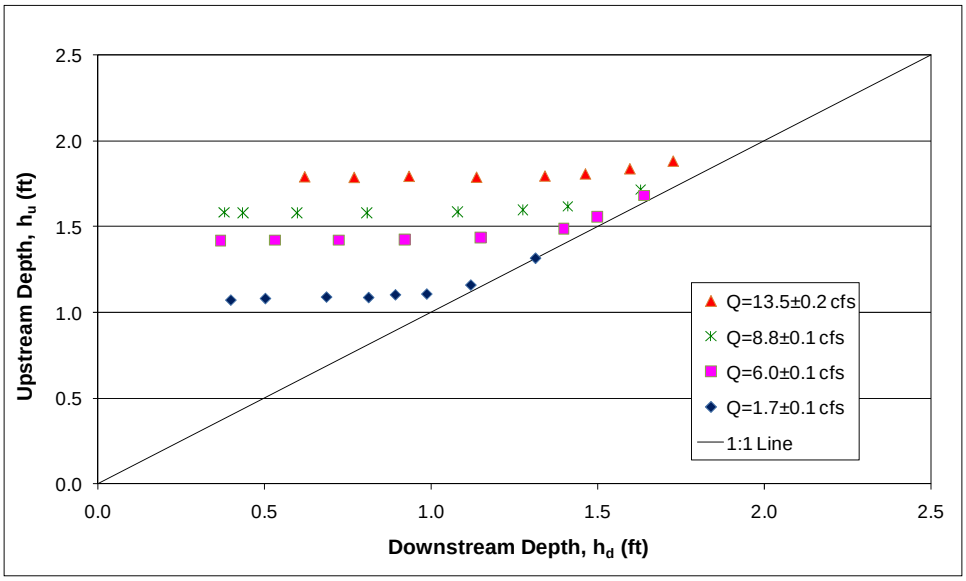

Figure 5.10 – LPCB Submergence Data

5.3.1 Villemonte Model

The resulting Villemonte Models are presented below in Figures 5.11-5.13. Also, the coefficient (m) for each of the barriers is listed below in Table 5.2, with the associated standard error. The model provides a reasonable fit to the data, and is more straightforward than the empirical model, which depends on the flow rate being known.

In order to obtain the coefficient value, the actual flow rate (Q) was measured, and the theoretical flow rate upstream (Q_1) was calculated using the rating curve model already developed, with the measured height of water upstream. The only other parameters in the Villemonte model are the energy upstream and downstream, which are also being measured. With these measured values, the Microsoft Excel Solver function was utilized to select values for the coefficient (m) such that the standard error between the measured values of the submergence ratio and the model derived submergence ratio was minimized.

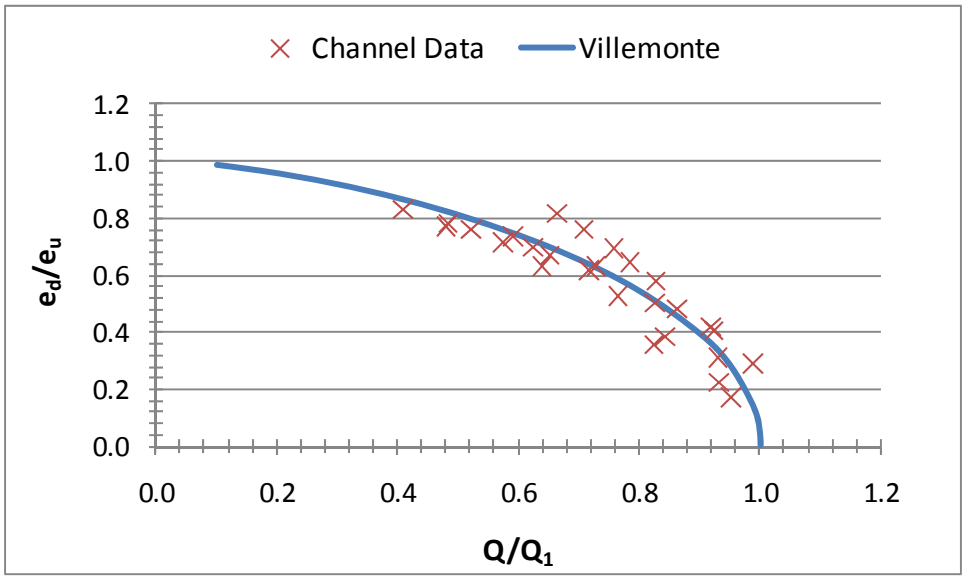

Figure 5.1 – MSSCB Submergence Model (Villemonte)

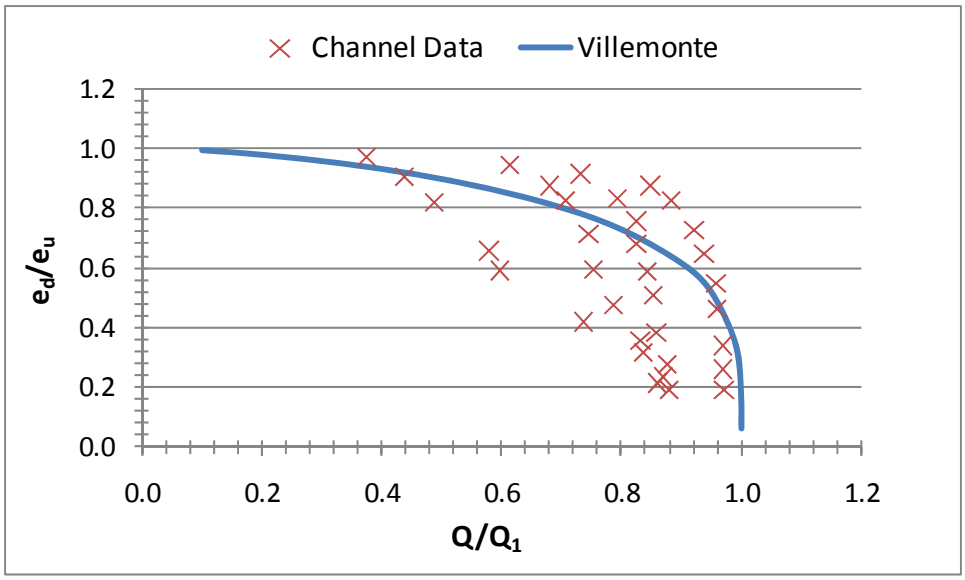

Figure 5.12 – CSB Submergence Model (Villemonte)

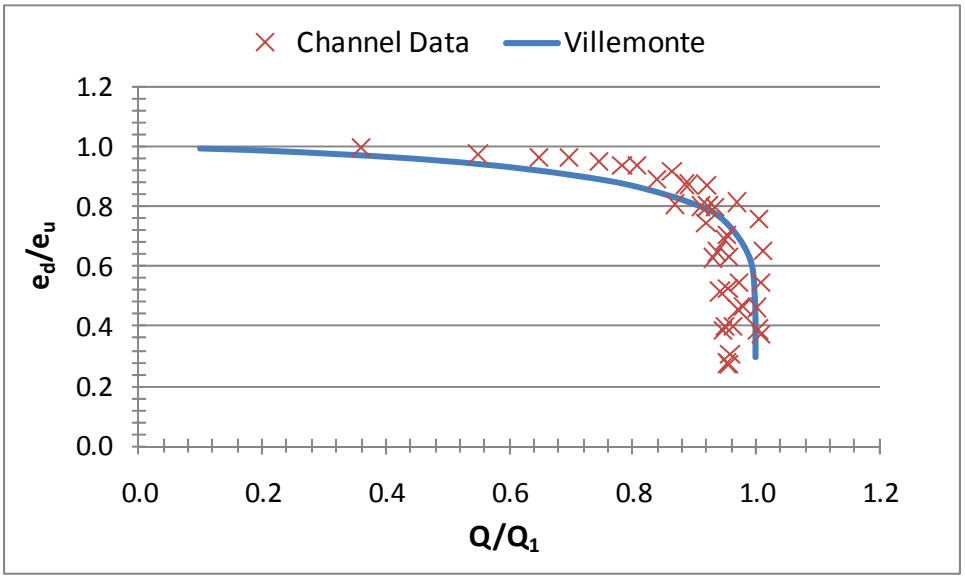

Figure 5.13 – LPCB Submergence Model (Villemonte)

Table 5.2 –Villemonte Model Coefficient Values

	MSSB	CSB	LPCB
m	0.485	0.255	0.109
S.E.	6.62%	12.12%	5.89%

Figures 5.14-5.16 are the graphical representations of the difference between the predicted submergence ratio and the data. The one to one line inserted on the graph has been inserted so a quick comparison of the difference between the modeled value and measured value can be made. If a data point lies on the line, this means that the modeled and measured values are the same. Conversely, the further away a data point is from the one to one line, the larger the discrepancy between the modeled and measured values. Furthermore, the data points have been separated by flow rate, to present the difference in error for different flow values.

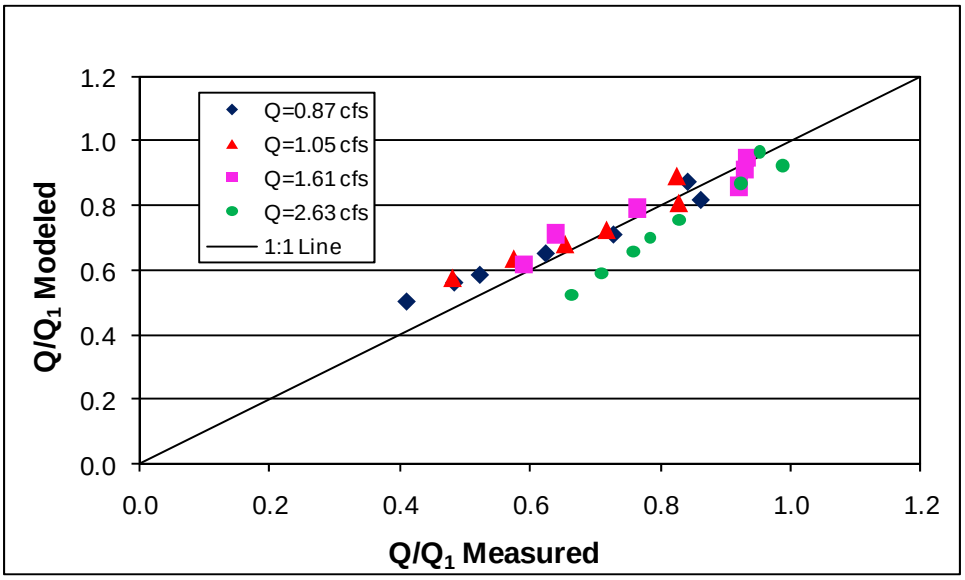

Figure 5.14 – MSSCB Villemonte Model Prediction Variation

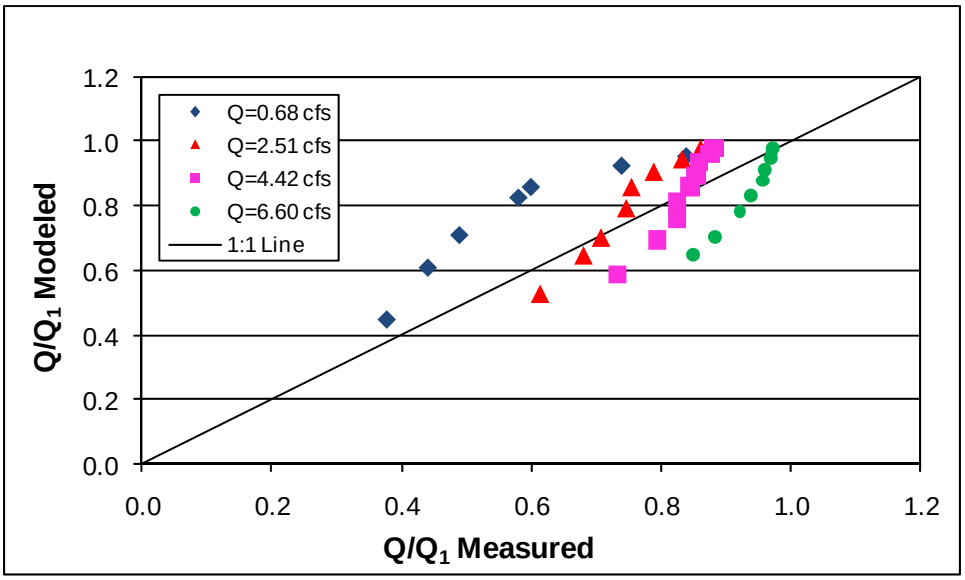

Figure 5.15 – CSB Villemonte Model Prediction Variation

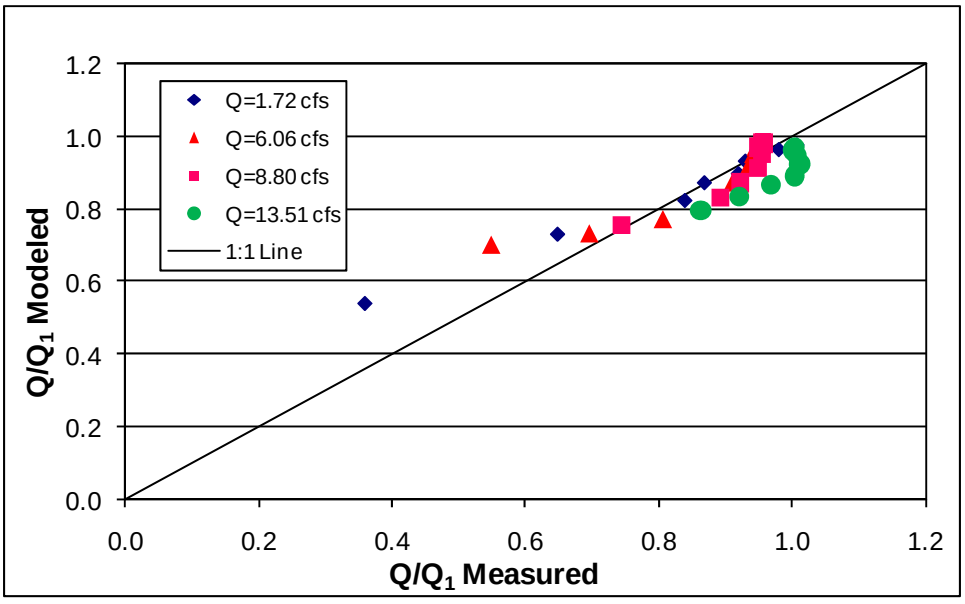

Figure 5.16 – LPCB Villemonte Model Prediction Variation

5.3.2 Empirical Model

The resulting Empirical models are given below in Figure 5.17-5.19, where a series of curves have been developed using the average of the four different flow rates that were used in the different experiments. The coefficient (B) is also listed below in Table 5.3. The process for obtaining this coefficient is same as used for the Villemonte model, with the exception that the Empirical submergence equation was utilized.

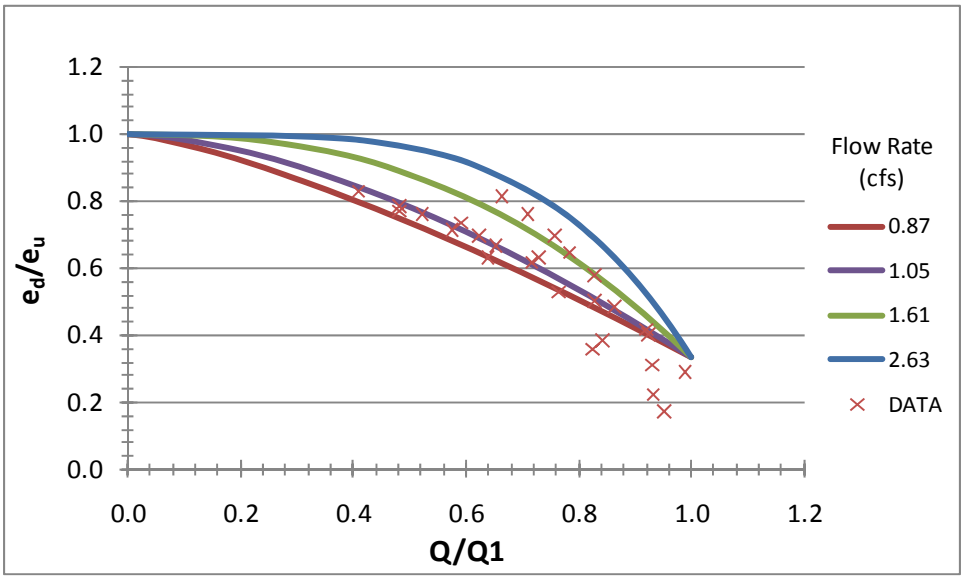

Figure 5.17 – MSSCB Empirical Submergence Model

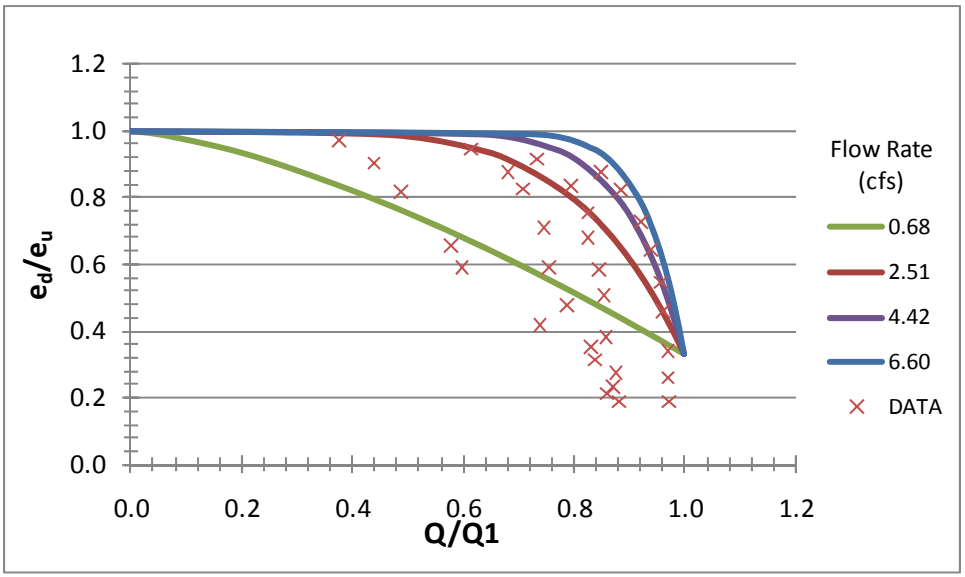

Figure 5.18 – CSB Empirical Submergence Model

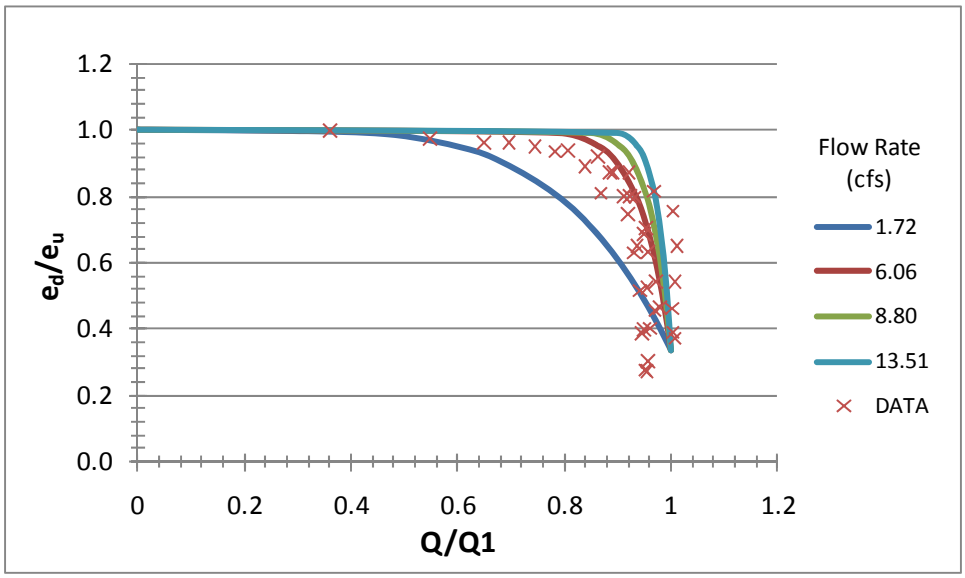

Figure 5.19 – LPCB Empirical Submergence Model

Table 5.3 –Empirical Model Coefficient Values

	MSSB	CSB	LPCB
B	100.93	97.690	63.194
S.E.	7.82%	11.87%	7.69%

Figures 5.20-5.21 below are the graphical representation of the difference between the Empirical model's predicted submergence ratio and the data. These graphs are similar to Figures 5.14-5.16, which were constructed for the Villemonte model, and are meant to highlight the difference in error for different flow values.

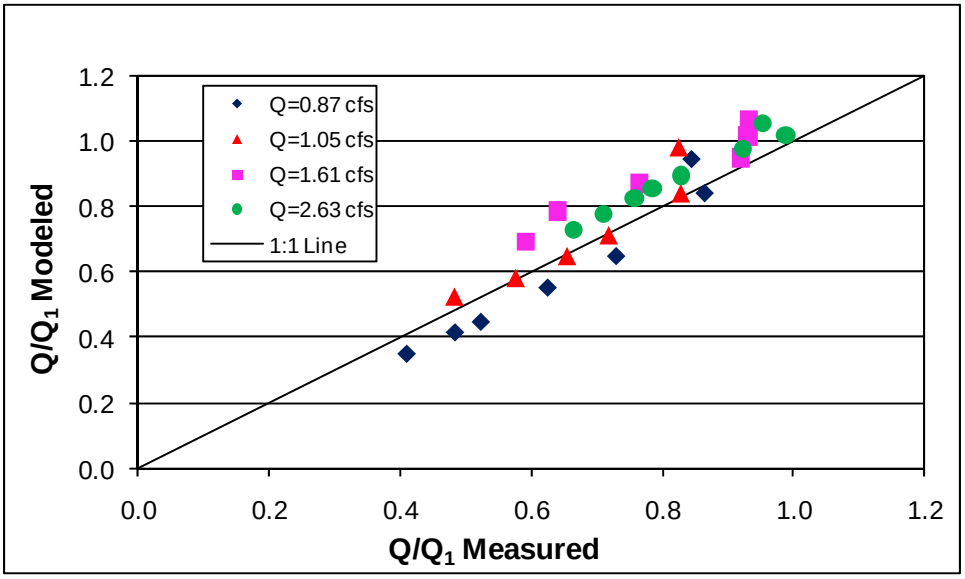

Figure 5.20 – MSSCB Empirical Model Prediction Variation

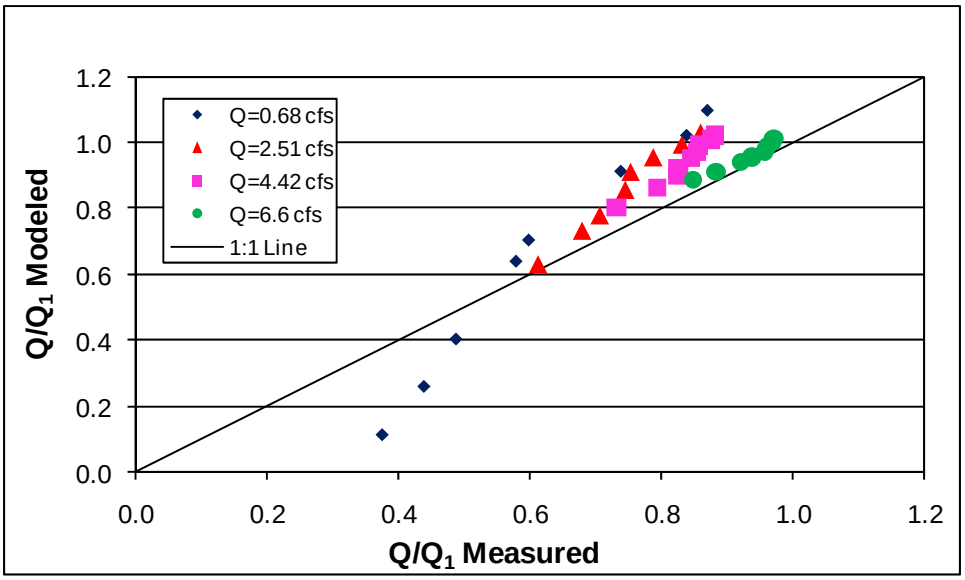

Figure 5.21 – CSB Empirical Model Prediction Variation

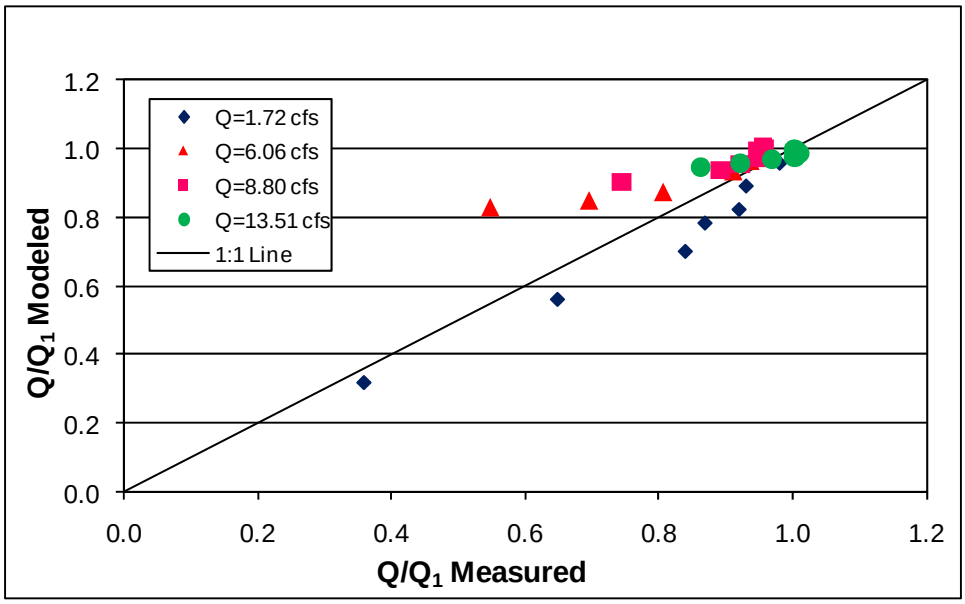

Figure 5.22 – LPCB Empirical Model Prediction Variation

5.3.3 Comparison of Submergence Models

A comparison of the standard errors between the Villemonte and Empirical models reveals that the Villemonte model represents the data more concisely for the MSSCB and LPCB. It can also be seen that the Empirical model represents the CSB more accurately, because of the lower standard error. However, the standard errors between the two models are very similar. Because the errors are comparable and the use of the Villemonte model is more straightforward (not dependent on the flow rate), the use of this model should be the preferred choice when modeling the affect that downstream submergence will have on rating curve. Furthermore, the fact that the Villemonte model describes submergence so well is due to the fact that it was developed for weir structures, which each of the TCTBs approximate with their small orifice sizes. However, the Empirical model did relatively well in its prediction, but is better suited to modeling flow through barriers where the fraction of open space is larger and the flow through the orifice will have more of an impact.

Chapter 6

Clogging Evaluation

6.1 INTRODUCTION

When considering the hydraulic performance of a TCTB, clogging of the drainage opening should be considered. This is because the small openings in the barriers will make them more susceptible to clogging. If the barrier becomes clogged, the specific energy upstream will increase as a function of the amount of clogging until the drainage opening is completely clogged. After the opening is completely clogged, the barrier will then exhibit flow characteristics similar to a weir.

In order to study the effect that a variable amount of clogging would have on the hydraulic performance of a TCTB, the modified single slope barrier (MSSCB) was tested. This barrier was equipped with a device that closed off part of the open space and allowed testing to be performed at 50% and 75% of the original drainage opening area. The original MSSCB can be seen in Figure 6.1 and the barrier when 50% and 75% clogged can be seen in Figures 6.2 and 6.3 respectively.

Figure 6.1 – Original MSSCB with no Clogging

Figure 6.2 –MSSCB 50% Clogged

Figure 6.3 –MSSCB 75% Clogged

Testing of this barrier in all three conditions was conducted as described in Section 3 of this paper. The next sections will describe the experimental results and the conclusions that can be drawn from those results.

6.2 EXPERIMENTAL RESULTS

When clogging occurs, it changes the fraction of open space that is available to the barrier. Since the fraction of open space is a variable in the equations for Type 1,2, and 3 flow, it should be possible to adjust this parameter to account for a desired amount of clogging. Before the experiments on the MSSB were conducted, the fraction of open space was adjusted to represent the 50% and 75% clogged condition. This was done by simply multiplying the original fraction of open space by the percentage of open space available after clogging, $F_o * (1 - \%\text{clogged})$. With this variable changed and all others left the same Figure 6.4 was developed. From this graph it can be seen that as the percentage of clogging increases the equations will shift to closer to the ordinate axis, and that if complete clogging were to occur, weir type flow would be developed.

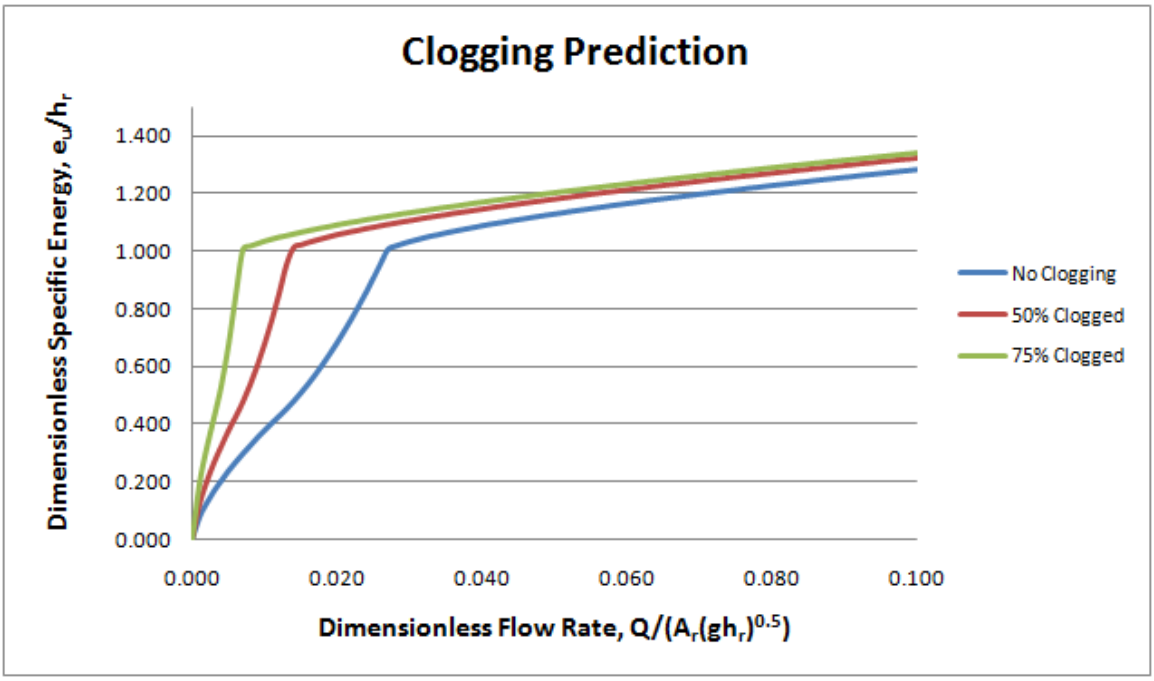

Figure 6.4 –MSSB Clogging Prediction

Next, in order to determine if this prediction adequately predicts the effects of clogging, the model was compared to the experimental data. This data is displayed below, in Figure 6.5, along with the prediction curves that were displayed in Figure 6.4. It can be seen from the graph that the prediction follows the general trend in the data. The standard error in the prediction is presented in Table 6.1.

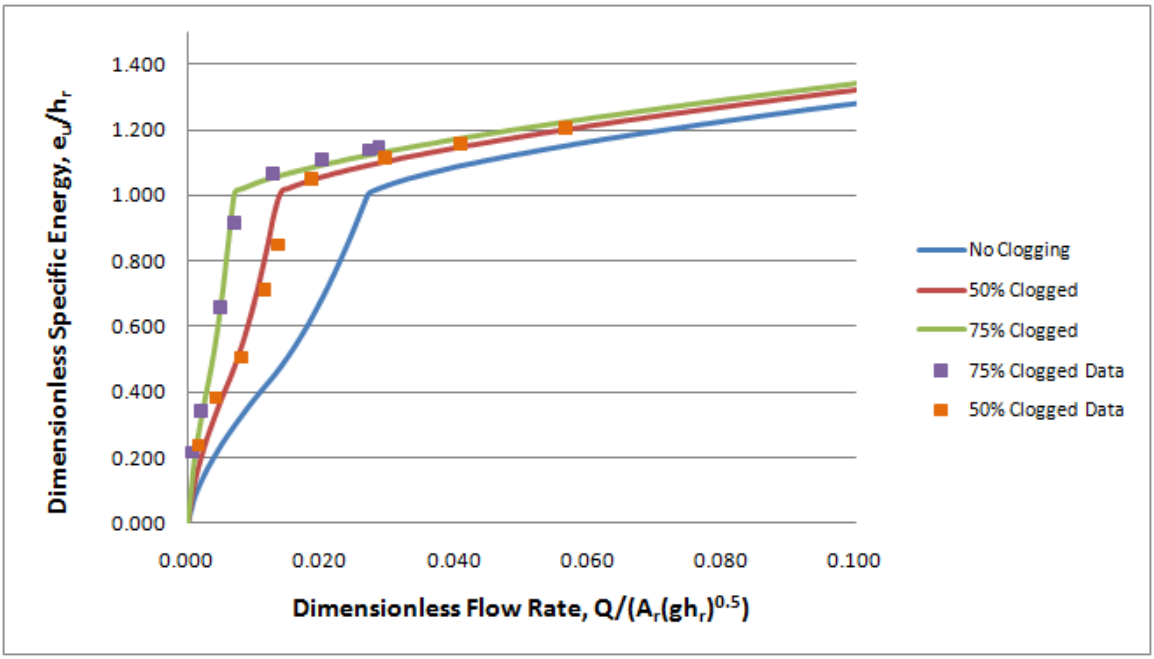

Figure 6.5 –MSSB Clogging Prediction Results

Table 6.1 – Standard Error of Clogging Prediction

% Clogged	S.E.
50%	6.78%
75%	4.20%

With these results, it is now possible for designers to determine the effects that various amounts of clogging will have on the hydraulic rating curve of a barrier being considered, by simply changing the fraction of open space to account for the clogged condition. Furthermore, this information can also be used by designers in order to design barriers with different sized openings to meet the hydraulic characteristics in a particular area.

Lastly, as was mentioned earlier in Section 3.2.1, this makes possible the creation of a rating curve to describe the SSCB and SSCB-SPL. By using the same coefficients

already derived for the MSSB and changing the fraction of open space to match that of each barrier, a rating curve can be created. These rating curves are presented below in Figure 6.6. The MSSCB barrier has also been included for comparison purposes. Furthermore, the parameters used to create these models are included below in Table 6.2.

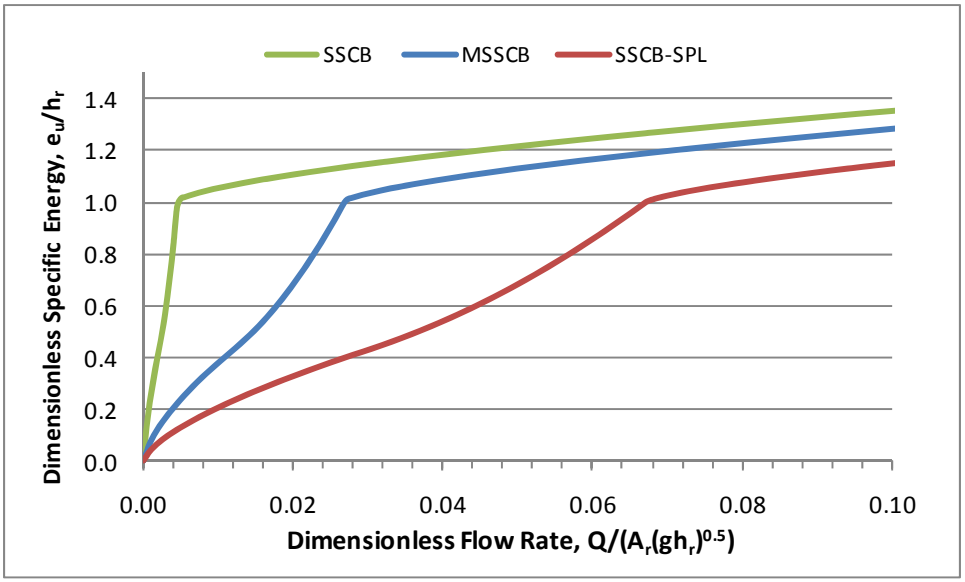

Figure 6.6 –SSCB Rating Curve

Table 6.2 – SSCB/SSCB-SPL Rating Curve Parameters

TCTB	C_b	C_c	C_d	F_o
SSCB	0.588	1.000	0.843	0.635%
SSCB-SPL	0.588	1.000	0.843	9.52%

Chapter 7

Modeling in HEC-RAS

7.1 INTRODUCTION

When designing highway drainage structures such as culverts and bridges, the hydraulic modeling software HEC-RAS (Hydrologic Engineering Center-River Analysis System) is often used in order to determine the water elevation that will result for various flows. Currently, if the water elevation overtops the roadway, the program can be set to calculate the flow using the pressure/weir method. In this calculation, the standard broad crested weir equation is used with a recommended value of 2.6 for the weir coefficient. However, when an obstruction such as a Temporary Concrete Traffic Barrier (TCTB) is placed on the roadway this coefficient will no longer will be applicable to describe that flow, because the barrier will act as an obstruction and will cause the upstream energy to increase compared to what would be calculated using the suggested weir coefficient. In order to model the effect that placing a barrier on the roadway will have, the weir coefficient can be modified to match an experimentally derived rating curve for the barrier that is going to be used. This section will explore how this can be accomplished by using two steady state example problems in HEC-RAS and the Concrete Safety Barrier (CSB (1)-04).

7.2 HYDRAULIC RATING CURVE

For the examples demonstrated in this chapter the CSB was selected as the barrier to be analyzed. The rating curve for this barrier has been reproduced below in Figure 7.1.

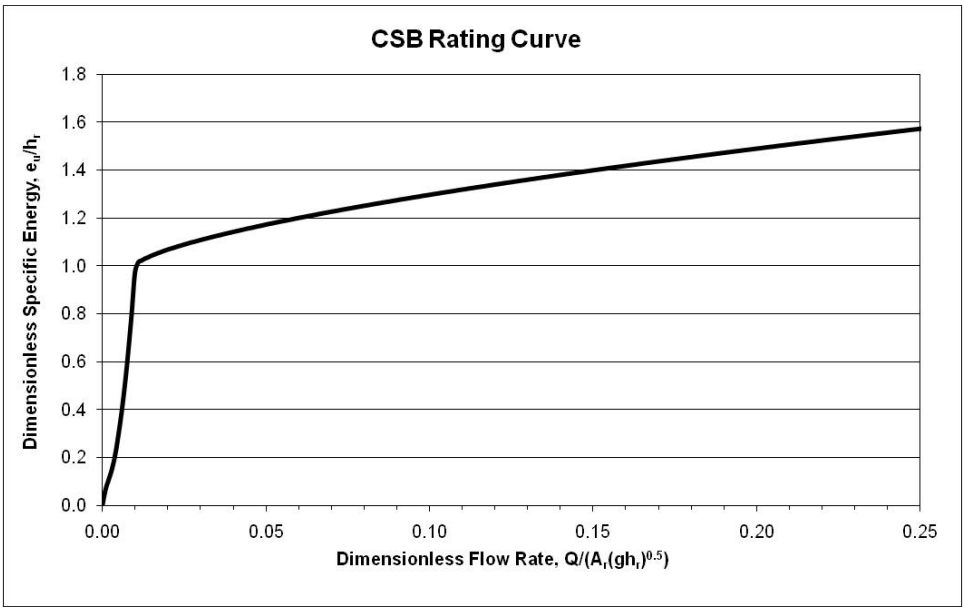

Figure 7.1 – CSB(1)-04 Rating Curve

This rating curve is non-dimensional because it was developed using a half scale model of the barrier, and the parameters needed to be non-dimensional in order to relate the model to the actual barrier. This however, is also advantageous for modeling in HEC-RAS, because the non-dimensional form allows for the easy calculation of the flow rate and energy upstream for varying widths of barriers by simply inserting the known values.

7.3 HEC-RAS EXAMPLES

Several example problems are included when HEC-RAS Version 4.0 is downloaded from the United States Army Corps of Engineers website (http://www.hec.usace.army.mil/software/hec-ras/). The two examples that this report will be using are the Single Bridge-Example 2 and ConSpan Culvert Example, which

may be found by searching the default project folder where HEC-RAS data is stored. In the Single Bridge-Example 2 simulation a simpler procedure by which a flat roadway surface will be evaluated, and in the ConSpan Culvert Example a procedure will be developed by which barrier placement on a sloped roadway can be modeled. A sample screenshot showing the two examples is show below in Figure 7.2.

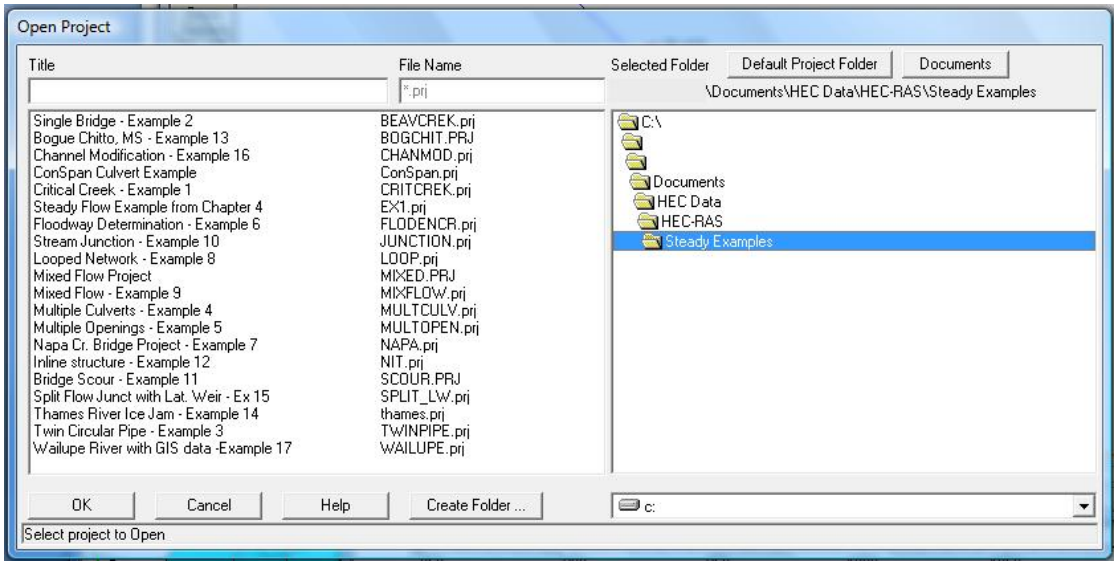

Figure 7.2 – HEC-RAS Open Project Screenshot

7.4 HEC-RAS SINGLE BRIDGE-EXAMPLE 2

In the HEC-RAS Single Bridge-Example 2, a bridge with a level deck is used to show how a horizontal roadway surface might be modeled. The procedure was developed as part of TxDOT Research Project 0-5492 presented by Charbeneau et al (2008). The procedure that this report uses for this example, however, can also be used to model the flow through a culvert with a horizontal roadway surface, because when modeling both structures the pressure/weir method is utilized. Furthermore, an iterative approach is

necessary to solve this problem because as the weir coefficient changes so will the weir flow rate.

In the procedure developed by Charbeneau et al. (2008) the non-dimensional rating curve will be used to determine the dimensional weir coefficient used in HEC-RAS. In order to do this the general weir equation, Equation 7.1, can be transformed into a non-dimensional form, Equation 7.2. In Equation 7.1 (Q) is the flow rate over the weir, (C) is the dimensional weir coefficient, (L) is the length of the weir and (H) is the height over the weir. In Equation 7.2 the general equation has been algebraically transformed to be in terms of the non-dimensional flow rate and non-dimensional energy used in the rating curve and (C_w) has been given the subscript w to denote that it is the non-dimensional coefficient. Furthermore, the energy upstream of the barrier (e_u), which is the total energy minus the elevation of the deck, has been substituted for (H).

$$Q = CLH^{1.5} \tag{7.1}$$

$$\frac{Q}{L\sqrt{g{h_r}^3}} = C_w \left(\frac{e_u}{h_r}\right)^{1.5} \tag{7.2}$$

By comparing the two equations it is possible to see that the relationship between the non-dimensional and dimensional coefficients is the square root of gravity. This relationship is shown below in Equation 7.3.

$$C = C_w\sqrt{g} \tag{7.3}$$

In the report by Charbeneau et al. (2008) the following procedure is outlined to solve the Single Bridge-Example 2 problem:

1. Run HEC-RAS with default weir coefficient C = 1.44 $m^{0.5}/s$ (2.6 $ft^{0.5}/s$), and obtain the flow rate over bridge deck (weir flow, Qweir, provided by RAS).
2. Nondimensionalize Qweir with length of bridge crest (L provided by RAS as difference between left and right weir stations) and barrier height, hr, using barrier of interest.
3. Obtain dimensionless upstream specific energy for given dimensionless weir flow rate using rating curve from Figure 7.1. (Note: This can also be done by using the Enon Visual Basic script included in the Appendix)
4. Determine dimensionless weir coefficient, Cw, using Equation 7.2.
5. Determine dimensional RAS weir coefficient, C, using Equation 7.3.
6. Re-run HEC-RAS with new weir coefficient C.
7. Repeat steps 1 through 6 until RAS weir coefficient converges, typically within one percent relative error from the previous iteration.

The first step in this procedure is to run a steady flow simulation in HEC-RAS using a weir coefficient of 2.6. Once this is accomplished, the Bridge Output screen (Figure 7.3) can be opened and the required values ascertained. For this analysis, the values that are needed are: Q_{weir}, Weir Sta Lt, and Weir Sta Rt.

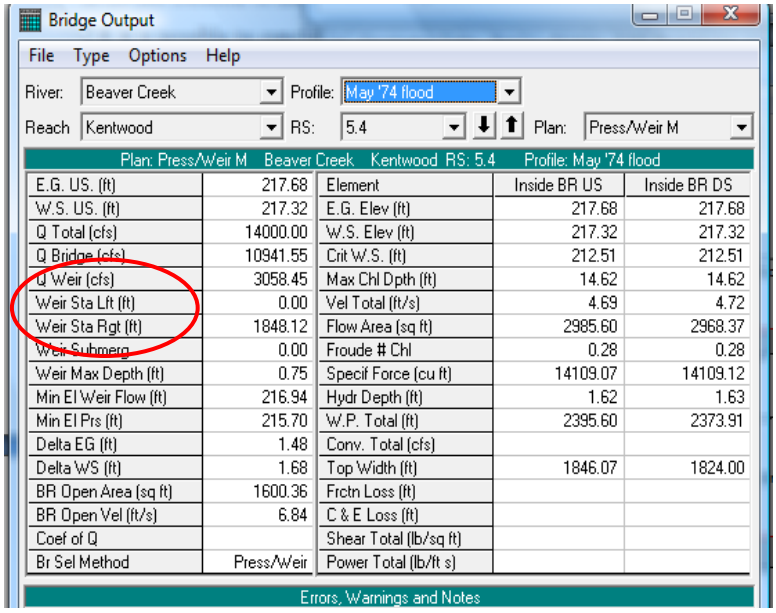

Figure 7.3 – HEC-RAS Bridge Output

The critical values for subsequent iterations are shown in Table 7.1. With these values, Steps 1 and 2 can be accomplished. For the analysis done in this memo, Step 3 was then completed by using the Enon function in Excel to calculate the non-dimensional energy predicted by the rating curve (value = 1.209). Now that the non-dimensional energy and non-dimensional flow rate have been calculated, Equations 7.2 and 7.3 can be used to calculate a new value for the HEC-RAS weir coefficient of 0.272. Table 7.2 below shows the results of this procedure for the seven iterations necessary in order for the weir coefficient to converge. By comparing the upstream energy (e_u) in the last iteration to that computed in the initial HEC-RAS run with a weir coefficient of 2.6, it is possible to conclude that placing the barrier on the bridge surface will result in an increase of energy of 2.26 ft and a corresponding decrease of 1811.02 cfs in the weir flow rate.

Table 7.1 – HEC-RAS Initial Summary

C	2.6
High Chord (ft)	216.93
U.S. E_u (ft)	217.68
U.S. e_u (ft)	0.75
Qweir (cfs)	3058.45
L (ft)	1848.12

3Table 7.2 – Single Bridge-Example 7 Iterations

		Iterations						
		1	2	3	4	5	6	7
(Step 1)	**Q_{weir} (cfs)**	3058.45	1767.03	1446.91	1329.54	1283.56	1258.47	1247.43
	L (ft)	1848.12	1849.16	1849.44	1849.54	1849.59	1849.61	1849.62
(Step 2)	**$Q/L(gh_r^3)^{0.5}$**	0.064	0.037	0.030	0.028	0.027	0.026	0.026
(Step 3)	**e_u/h_r**	1.209	1.131	1.108	1.099	1.096	1.093	1.093
	e_u (ft)	3.325	3.111	3.047	3.023	3.013	3.007	3.006
(Step 4)	**C_w**	0.048	0.031	0.026	0.024	0.023	0.023	0.023
(Step 5)	**C ($ft^{0.5}/s$)**	0.272	0.174	0.147	0.137	0.133	0.130	0.129

The final weir coefficient C = 0.129 $ft^{0.5}/s$ will likely appear too small. Typical weir coefficient values for use with Eq. (7.1) range from 2.5 to 3.1 (US Customary units), with the HEC-RAS default value C = 2.6. The apparent difficulty lies primarily with choice of datum. Standard application of HEC-RAS would take the top of the rail or barrier as the upper chord of the bridge. For this example with h_r = 2.75 ft, the high chord would be 216.93 + 2.75 = 219.68 ft. The head on this high chord corresponding to the final e_u value is $H = e_u - h_r$ = 0.256 ft. With the default weir coefficient, this standard application would give a weir discharge $Q_{weir} = C\,L\,H^{1.5}$ = 2.6 x 1850 x $(0.256)^{1.5}$ = 620 cfs, which is approximately half the magnitude calculated in this example. In order for a standard application of HEC-RAS to provide the results presented herein, a weir coefficient value $C = Q_{weir}/[L\,H^{1.5}]$ = 5.21 would need to be used, which is significantly

larger than the expected range of values. Based on this discussion it is concluded that a standard application of HEC-RAS will predict a larger upstream headwater (when typical weir coefficient values are used).

7.5 HEC-RAS CONSPAN CULVERT EXAMPLE

In this section, the procedure for solving the weir coefficient necessary to simulate placement of the CSB(1)-04 TCTB in the Single ConSpan Culvert Example will be presented. The main difference between this and the previous example is that the roadway is not flat and energy over the roadway is used to determine flow rate, rather than using the weir flow rate to determine the energy Similar to the Single Bridge-Example 2 procedure, this example uses an iterative approach in order to balance the flow rate and water elevation calculated in HEC-RAS with the values that are obtained using the data from the rating curve.

7.5.1 HEC-RAS Example Modifications

In the ConSpan Culvert Example a single barrel Conspan arched pipe is used to transmit water from one side of the roadway to the other. One modification is necessary to this example problem to ensure that weir flow is developed. The example problem comes preloaded with flow data corresponding to the 5, 10, 25, and 50 year floods. The greatest flow rate, which is 1000 cfs (50 year flood) doesn't result in water overtopping the roadway. For the example presented in this memo, a value of 2000 cfs was entered for the 50 year flood, which caused the water level to rise above the height of the roadway. An example screenshot of the modifications to the steady state flow data is shown in Figure 7.4.

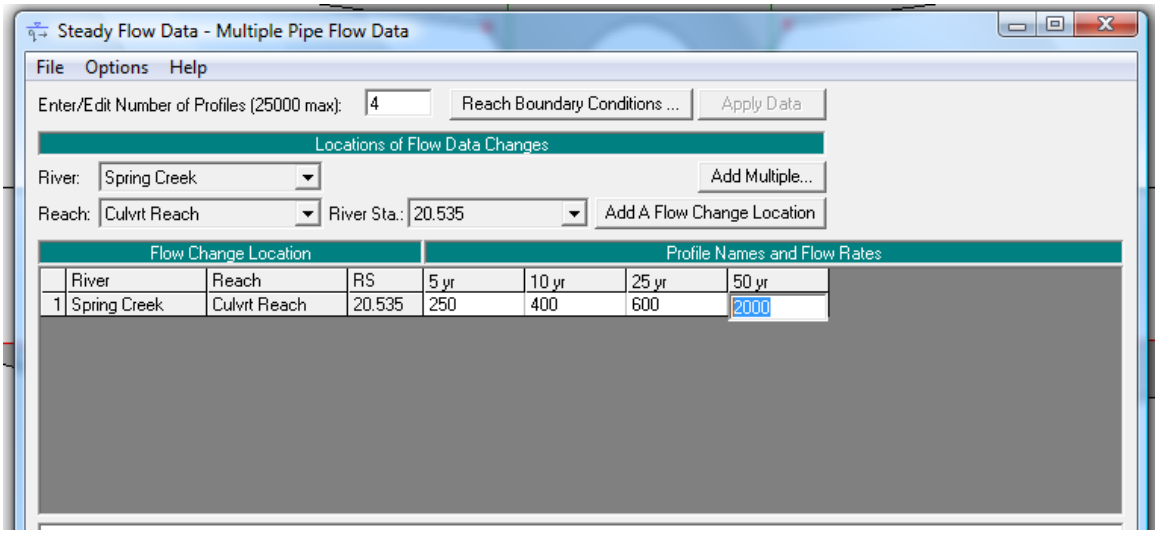

Figure 7.4 – HEC-RAS Example Flow Alteration

7.5.2 ConSpan Culvert Procedure

As stated earlier, in order to solve for the weir coefficient that describes the flow over a roadway with barriers, an iterative procedure must be used. The first step in this procedure is to obtain the flow rate over the roadway as if the barrier were not there. This is done by performing a steady flow simulation in HEC-RAS with the weir coefficient initially set to the recommended value of 2.6 (Note: This should be the default value already entered in the Conspan example.). After this analysis is completed, the culvert output table can be opened and the values needed for the subsequent calculations can be garnered. The culvert output for this analysis is presented below as Figure 7.5. The values that are of most importance in this table are: weir flow (Q Weir), the left and right limits of the weir flow (Weir Sta Lft/Rgt), and upstream energy (U.S. E.G.).

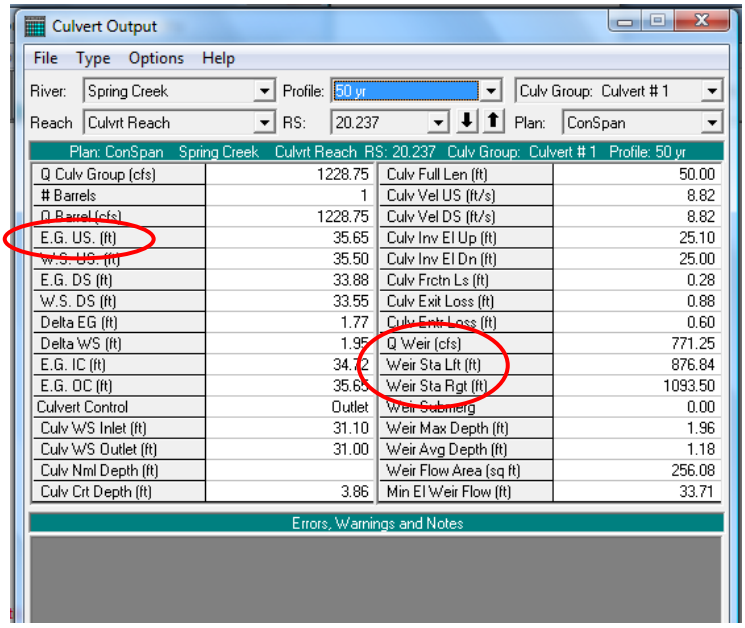

Figure 7.5 – ConSpan Culvert Output (C=2.6)

With these numbers it is then possible to perform the first iteration. In order to do this we must first approximate the roadway as a series of horizontal crested weirs. This is because the equation that describes the flow over a weir is based on flow over a horizontal surface; however, the roadway is sloped. For this example problem the roadway was broken into 5 equal length weirs, with outside of the outmost left and right weirs placed at the Weir Sta Lft and Weir Sta Rgt locations. Furthermore, the elevation of each weir approximation was taken to be the average of the left and right roadway elevations of each weir segment. Figure 7.6 below, shows the roadway cross-section, the weir approximation and the U.S. E.G. for the first analysis with the Weir Coefficient (C) equal to 2.6.

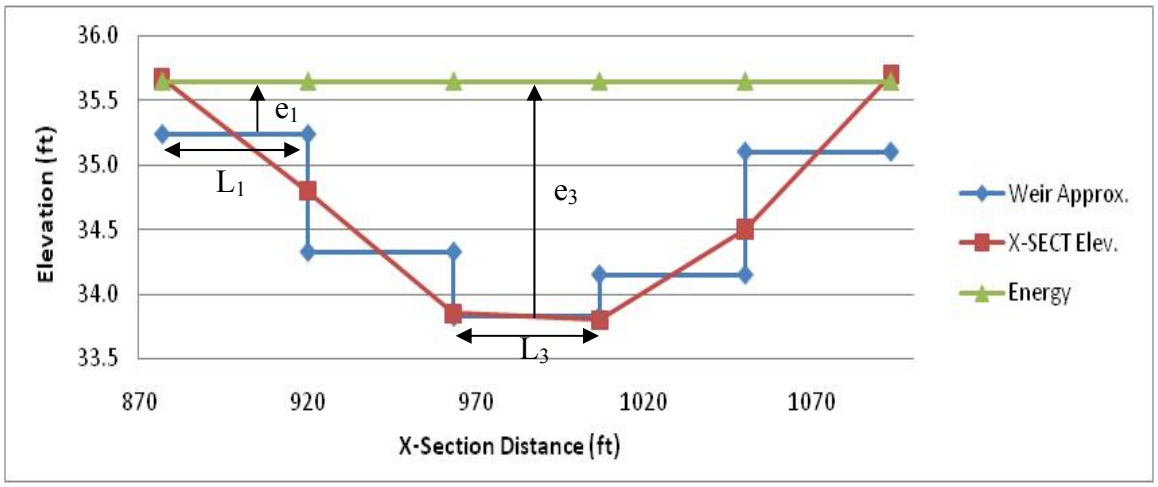

Figure 7.6 – Weir Approximations

Now that the roadway has been approximated as a set of horizontal weirs the following iterative procedure can be followed in order to determine the weir coefficient value:

1. Calculate the energy (e) over each section by subtracting the i^{th} weir elevation $(W.E.)_i$ from the U.S. E.G (Column 1 Table 7.3).
2. The next calculation (Column 2 Table 7.3) is then to convert this energy to the non-dimensional form used in the rating curve by simply dividing by the height of the barrier (h_r).
3. With the non-dimensional energy over each weir and the rating curve, it is then possible to find the non-dimensional flow (Column 3 Table 7.3) over each weir (Note: This can be done by simply interpolating from Figure 7.1 or by using the visual basic script provided in the Appendix).
4. Next, the flow rate (Column 4 Table 7.3) over each weir segment can be calculated by simply solving for the actual flow rate (Q) through substituting the known values (see appendix for values) into the non-dimensional equation.

5. Furthermore, a dimensional weir coefficient (Column 5 Table 7.3) can be calculated for each weir segment by rearranging the weir equation ($Q=CLH^{1.5}$, where H equals the energy (e_i) over the weir).
6. Finally, the value of the weir coefficient for the next iteration can be calculated by taking the average of the coefficients for each weir approximation.

An example of this calculation done in Excel is shown below in Table 7.3. It should be noted that the total weir flow rate (summation of column 4) is equal to 31.78 cfs, and that this value is less than 771.25 cfs, which was reported by HEC-RAS. The purpose of the subsequent iterations will be to determine a weir coefficient that accurately models the flow past the barrier based on the rating curve with a flow rate equal to the weir flow rate calculated in HEC-RAS.

Table 7.3 – ConSpan Calculations in Excel (1st Iteration)

							(1)	(2)	(3)	(4)	(5)
	length	Left STA	Right STA	X-SECT Elev. LT	X-SECT Elev.RT	Avg Elev	e_i	e_i/h_r	qnon	Q	C
	(ft)	(ft)	(ft)	(ft)	(ft)	(ft)	(ft)	(ft/ft)		(cfs)	($ft^{0.5}/s$)
L_1	43.3	876.8	920.2	35.67	34.80	35.24	0.41	0.151	0.003	3.18	0.274
L_2	43.3	920.2	963.5	34.80	33.85	34.33	1.33	0.482	0.007	7.47	0.113
L_3	43.3	963.5	1006.8	33.85	33.80	33.83	1.83	0.664	0.008	8.99	0.084
L_4	43.3	1006.8	1050.2	33.80	34.50	34.15	1.50	0.545	0.007	8.04	0.101
L_5	43.3	1050.2	1093.5	34.50	35.70	35.10	0.55	0.200	0.004	4.11	0.232
										Avg C	0.161
										Q	31.78

7.5.3 ConSpan Second Iteration

The procedure for the second iteration is the same as what was done in the first iteration with the exception that the weir coefficient used in HEC-RAS should now be set equal to 0.161. If this value is used, a culvert output similar to Figure 7.7 will be obtained. Using these values and the procedure employed in the first iteration, a new weir coefficient value of 0.265 should then be attained along with a total flow rate of 515.14 cfs. An example of the calculations completed for the second iteration is shown below in Table 7.4.

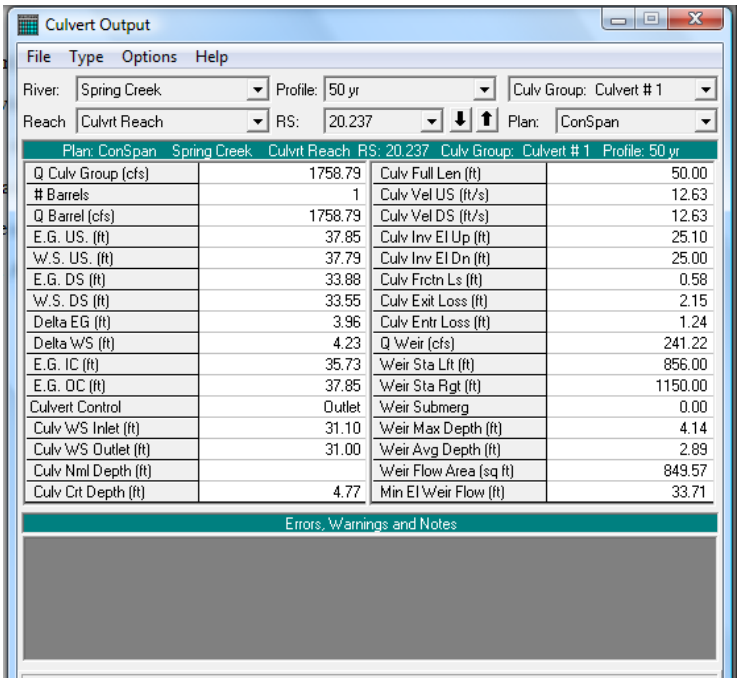

Figure 7.7 – ConSpan Culvert Output 2 (C=0.161)

Table 7.4 – ConSpan Calculations in Excel (2nd Iteration)

	length (ft)	Left STA (ft)	Right STA (ft)	X-SECT Elev. LT (ft)	X-SECT Elev.RT (ft)	Avg Elev (ft)	(1) e_i (ft)	(2) e_i/h_r (ft/ft)	(3) qnon	(4) Q (cfs)	(5) C ($ft^{0.5}/s$)
L_1	58.8	856.0	914.8	36.10	34.80	35.45	2.4	0.87	0.009	14.21	0.065
L_2	58.8	914.8	973.6	34.80	33.90	34.35	3.5	1.27	0.090	136.65	0.355
L_3	58.8	973.6	1032.4	33.90	33.70	33.80	4.1	1.47	0.191	290.89	0.607
L_4	58.8	1032.4	1091.2	33.70	35.70	34.70	3.2	1.15	0.041	62.91	0.191
L_5	58.8	1091.2	1150.0	35.70	37.20	36.45	1.4	0.51	0.007	10.47	0.108
										Avg C	0.265
										Q Tot	515.14

7.5.4 ConSpan Results

A graph of the results of the first four iterations is presented below in Figure 7.8. After four iterations it can be seen that a solution converges around a weir coefficient value of 0.246. At this value the flow rate and water elevations developed in HEC-RAS and by the rating curve produce similar results. The final flow rate over the roadway and the upstream energy can then be calculated by inserting a value of 0.246 for the weir coefficient in HEC-RAS. The result is a flow rate of 311.07 cfs and an upstream energy at the barrier of 37.51 ft. The original flow rate calculated without the barrier placement was 771.25, and the upstream energy was 35.65 ft. By placing the barrier, the flow rate over the roadway will then decrease by 460.18 cfs and the upstream energy will increase by 1.86 ft.

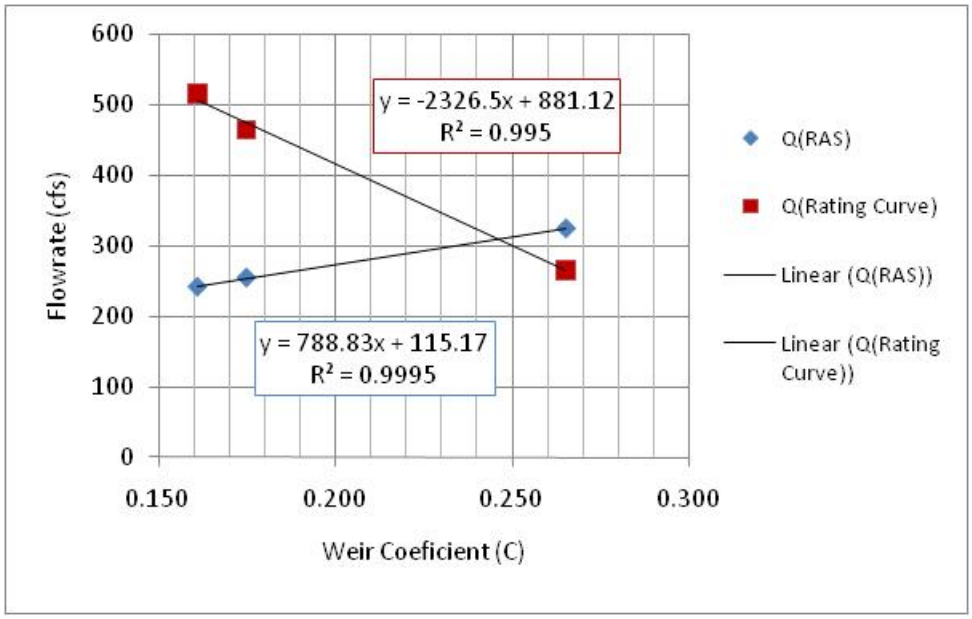

Figure 7.8 – Plot of Calculated Flow Rates vs. Weir Coefficients

7.5.5 Conclusions

This chapter has shown that it is possible to modify the weir coefficient value in HEC-RAS in order to hydraulically model the placement of a concrete traffic barrier on the roadway surface. To do this, an iterative procedure must be used. Two example problems, the Single Bridge-Example 2 and ConSpan Culvert have been demonstrated with the Concrete Safety Barrier (CSB(1)-04) in this memo. In the Single Bridge-Example 2 procedure an increase in the upstream energy of 2.25 ft and a decrease in the weir flow rate of 1811.02 cfs occurred as a result of barrier placement. Furthermore, through the ConSpan example it can be seen that placing the barrier on the roadway will result in the upstream energy increasing by 1.86 ft and the flow rate decreasing by 460.18 cfs.

Chapter Eight

Summary and Conclusions

8.1 PROBLEM SUMMARY

Temporary Concrete Traffic Barriers (TCTBs) are essential in order to protect the traveling public from entering potentially hazardous locations. To do their job well, a large mass and low center of gravity is needed to resist the energy of a vehicular impact. To maximize these two attributes barriers need to be constructed with the smallest possible drainage opening. This is because the drainage openings, which are located at the bottom of a barrier, decrease the total mass and shift the center of gravity higher. This then leads to barrier designs with small drainage openings. If a barrier is then placed in a location where flooding is an issue, the barrier could impact the local floodplain elevation due to the barrier acting as an obstruction to flow. This report explores how this impact is quantified by developing a hydraulic rating curve for four different barriers and providing an example of how barrier placement can be modeled in the hydraulic modeling software HEC-RAS.

8.2 CONCLUSIONS

Four main objectives were identified at the beginning of this research. The first was the development of a rating curve that sufficiently describes the relationship between upstream energy and flow rate under conditions where there is no downstream submergence and no clogging of the drainage opening. This research has resulted in the development of a rating curve for four standard TCTBs: the SSCB, SSCB-SPL, CSB, and

LPCB. To accomplish this, modeling was performed based on previous research presented by Charbeneau et al. (2008). This model proved to fit the experimentally derived data quite well, but is limited to modeling barriers in which experimental data has been obtained. This is because the model equations contain three coefficients which can only be obtained through fitting the model to the data.

The second objective was to determine the effect that downstream submergence will have on the rating curves. To accomplish this goal two models were utilized, both of which are presented by Charbeneau et al. (2008): the Villemonte Model and the Empirical Model. Both models require physical modeling in order to derive a single coefficient term. The Villemonte Model, which is an adaptation from earlier research (Villemonte, 1947), is independent of the flow rate. The Empirical Model developed in the paper by Charbeneau et al. (2008), however, is dependent on the flow rate. Both models have similar accuracy, with the Villemonte Model being the easiest and most straightforward to use. Therefore, when modeling the effect of submergence for the four barriers selected in this research, the Villemonte Model is the clear choice to be used.

The third objective of this research was to assess the effect that clogging of the drainage opening will have on the rating curve. Before any research was conducted, it was hypothesized that a simple change to the fraction of open space (F_o) in the rating curve model equations would result in the modeling of a barrier with varying degrees of clogging. This is because the F_o describes the area of the drainage opening, and when the drainage opening becomes clogged this number will be reduced. To test this hypothesis, the MSSCB was fitted with a device that allowed the area of the drainage opening to be adjusted. Two scenarios were tested, one with the barrier's drainage opening 75% clogged and the other with it 50% clogged. This research showed that when the F_o was

adjusted to represent the two clogged conditions the model fit the experimental data quite well. This now allows for the prediction of a rating curve for varying amounts of clogging by simply manipulating the F_o in the model rating curve equations.

The fourth and final objective of this research was to develop a procedure by which the TCTB rating curve data could be used in the hydraulic modeling software HEC-RAS, in order to model the placement of barrier on a roadway surface. To accomplish this, two example problems were considered. The first consists of a flat roadway surface and the second is a roadway with a vertical curve. In order to solve these problems the weir coefficient that HEC-RAS uses as part of the pressure/weir method can be altered in order simulate the placement of a barrier on the roadway.

The flat roadway example was developed as part of the research by Charbeneau et al. (2008). In this first example, the weir flow rate can be used with the rating curve to determine the energy upstream of the barrier. This then makes possible the calculation of a new weir coefficient to be input in HEC-RAS. The flat roadway problem is much easier to solve than the vertical curve problem, because the roadway does not have to be approximated as a series of horizontal weirs. The horizontal weir approximation is necessary when dealing with a vertical curve, because the water depth over the roadway surface changes as the roadway elevation changes. Therefore, horizontal weir approximations must be used to calculate the energy over each approximation. With the energy over each weir approximation and the rating curve, a flow rate can be obtained for each approximation and a new average weir coefficient calculated as an input to HEC-RAS. This research has shown through these two examples that it is possible to modify the weir coefficient in HEC-RAS in order to simulate the placement of a barrier on either a flat or vertically curved roadway surface.

Appendix A

A.1 QNON (NON-DIMENSIONAL FLOW RATE) VISUAL BASIC SCRIPT

```
Function Qnon(e, fo, a, cb, cc, cd)
  If (e < 1.5 * cc * a) Then
    Qnon = cb * fo * (1 / a) * (2 * e / 3) ^ 1.5 'Type 1 Flow'
  Else
    Qnon = cb * cc * fo * Sqr(2 * (e - cc * a)) 'Type 2 Flow'
  End If
    If e > 1 Then
    Qnon = Qnon + cd * (2 / 3 * (e - 1)) ^ 1.5 'Type 3 Flow'
  End If
  End Function
```

$e=e_i/h_r$
f_o=fraction of open space
$a=h_{rl}/h_r$
cb=horizontal contraction coefficient
cc=vertical contraction coefficient
cd=weir flow coefficient

A.2 ENON (NON-DIMENSIONAL ENERGY) VISUAL BASIC SCRIPT

```
Function Eguess(Q, fo, a, cb, cc, cd)
   If Q < cb * cc ^ 1.5 * fo * Sqr(a) Then
      Eguess = 1.5 * (Q * a / (cb * fo)) ^ (2 / 3)
   Else
      Eguess = ((Q / (cb * cc * fo)) ^ 2) / 2 + cc * a
   End If

End Function

Function Enon(Q, fo, a, cb, cc, cd)
  Eps = 0.0001
  Q_t = 0#

  Emax = Eguess(Q, fo, a, cb, cc, cd)
  emin = 0#

  Do While Abs(Q - Q_t) > Eps
    etest = (Emax + emin) / 2
    Q_t = Qnon(etest, fo, a, cb, cc, cd)
    If Q_t < Q Then
      emin = etest
    Else
      Emax = etest
    End If
  Loop

  Enon = etest
End Function
```

Q=non-dimensional flow rate, $\frac{q}{\sqrt{g h_r^{\,3}}}$

A.3 TCTB STANDARD DRAWINGS (TXDOT, 2009)

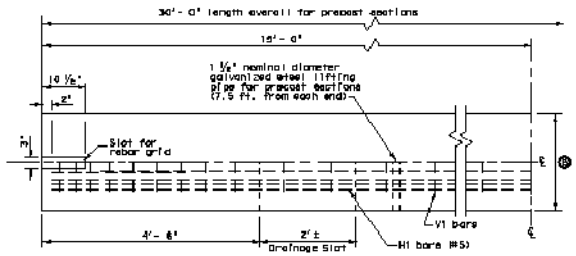

PLAN VIEW

(SYMMETRICAL ABOUTCENTER LINE)

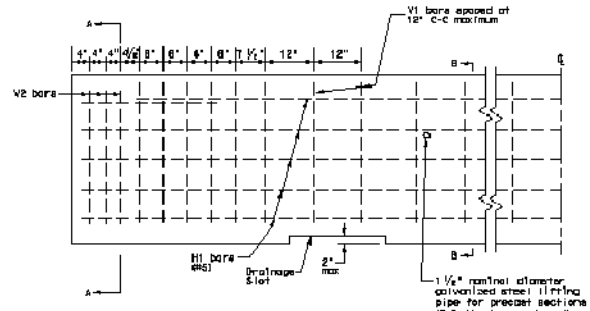

ELEVATION

(SYMMETRICAL ABOUT CENTERLINE)

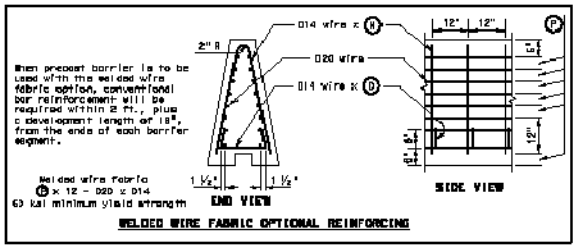

WELDED WIRE FABRIC OPTIONAL REINFORCING

GENERAL NOTES

1. Precast barrier length shall be 30 feet (±1") unless otherwise specified in the plans. Cast-in-place or slip-formed barrier shall have an intermediate barrier joint at a maximum spacing of 100 feet unless otherwise directed by the Engineer. Refer to the intermediate barrier joint detail. Cast-in-place or slip-formed barrier will have the vertical V1 bars placed at 12" C-C maximum except near joints. The narrower vertical bar spacing at the ends of each barrier segment, as shown in the elevation view, will be required at the joints. The V2 bars shown in the elevation view will be replaced by V1 bars for cast-in-place or slip-form construction.
2. The usual temporary installation will require the placement of the rebar grid in the ungrouted slot. The usual permanent installation using precast barrier will connect the barrier segments with the rebar grid placed in the slot and grouted in place.
3. When installed in a permanent roadway location, the end connections of the precast barrier shall be grouted with a mixture of two parts sand and one part cement with enough water to make the mixture plastic. Grouting shall be done in a manner that will assure a smooth surface at the joint.
4. All concrete shall be class C or H, unless otherwise specified.
5. All reinforcing steel shall be Grade 60, unless otherwise specified.
6. Each precast barrier to be installed in a temporary location shall be delivered with a rebar grid.
7. Chamfer top and end edges ¾ inch.
8. Unless otherwise shown in the plans, the Contractor has the option of placing either precast or cast-in-place permanent concrete barrier. Cast-in-place barrier may be slip-formed. Additional reinforcement may be field welded to the upper two-thirds of the reinforcing cage to provide bracing. Lifting pipe, rebar grid and slot shall be omitted for cast-in-place or slip-form construction.
9. Bar splices for roadway barrier shall be a minimum of 24 times the nominal diameter of the bar.
10. Welded wire fabric may be used as an option to conventional reinforcement for precast or cast-in-place barrier. Welded wire fabric shall be made in accordance with ASTM A 497.
11. Conduit will be provided only when called for elsewhere in the plans. The position of the conduit or conduit passageway may be adjusted to facilitate construction, subject to approval of the Engineer.
12. Transitions to barrier height, as needed, shall be determined by the Engineer. Changes in barrier height should not normally exceed 2 inches per 30 foot. Vertical steel shall be uniformly transitioned throughout the variation in barrier height as directed by the Engineer.
13. A 36 inch minimum height differential between top of barrier and top of ACP shall be required at placement in order to allow for up to 6 inches of future overlays while maintaining a 30 inch minimum future effective height of barrier. Total minimal barrier height for design is therefore dictated by allowance for future overlays plus existing shoulder step dimension "S". Minimums typically rounded to 42", 48" or 54" to facilitate precasting.

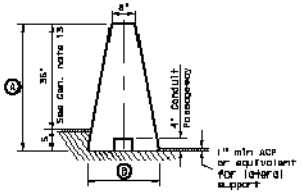

TYPICAL SECTION

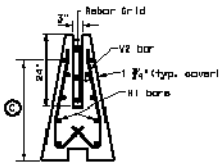

SECTION A-A

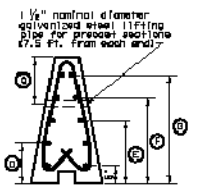

SECTION B-B

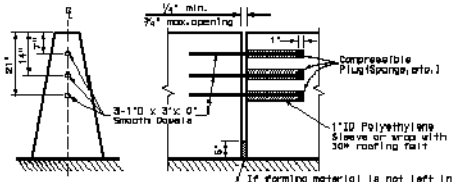

INTERMEDIATE BARRIER JOINT DETAIL (cast-in-place or slip-formed sections)

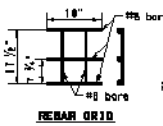

REBAR GRID

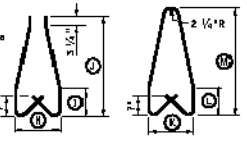

V2 BAR (#4) **V1 BAR (#4)**

REINFORCING DETAILS

R = Radius
D = Diameter

Barrier Height	DIMENSIONS (inches)															
A	B	C	D	E	F	G	H	I	J	K	L	M	N	O	P	Q
42	24	33 ½	13 ½	21	38 ½	36	15	9 ¼	33 ¼	15	9 ⅛	36	72	26	4	19 ½
48	26 ½	39 ½	15	24	33	42	17 ¼	10 ¾	38 ¼	17 ¼	10 ¾	42	84	31 ½	5	17
54	28 ⅞	45 ½	16 ½	27	37 ½	48	19 ½	12 ¼	45 ¼	19 ½	12 ¼	48	96	34 ¾	6	18 ½

Texas Department of Transportation
Design Division (Austin)

SINGLE SLOPE CONCRETE BARRIER
TYPE 2

SSCB(2)-00A

FILE: sscb00a.dgn	DW: CTH	CK: GTB	DW: BGD	CK: TRN	
© TXDOT MAY 1998	DIST	FEDERAL AID PROJECT			SHEET
REVISIONS					
	COUNTY		CONTROL	SECT	JOB	HIGHWAY

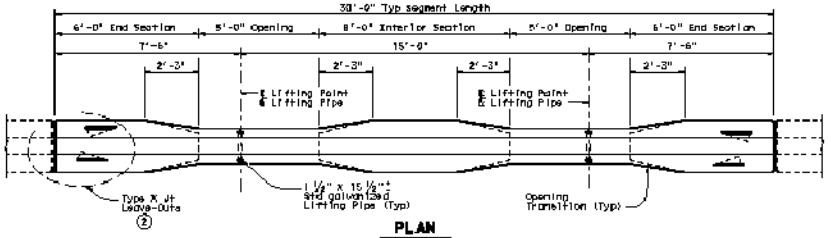

PLAN

Showing structural dimensions.

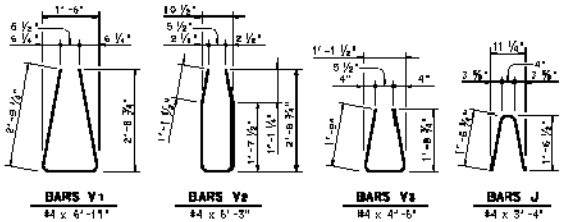

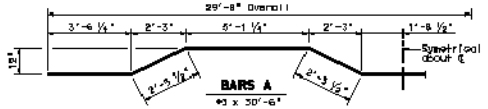

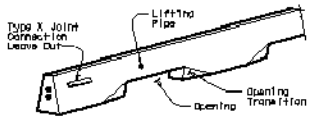

PARTIAL ISOMETRIC

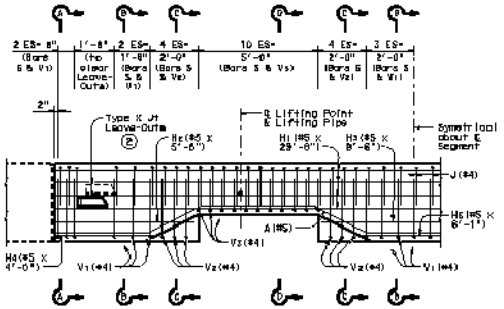

HALF ELEVATION

showing reinforcing.

SPECIAL LIFTING NOTES:

Barrier lifts shall be made with a two-point pick system, using either the lifting pipes or other method centering on the lifting points as detailed. In order to ensure that lifting forces are vertical and not inclined, two-point pick systems using cables require the use of a spreader beam or strong back. Due to structural limitations of the barrier unit, single-point pick systems at the center of the barrier unit are NOT permitted.

(1) A 3% draft, at the Contractor's option so as to ease form removal, is permitted at the top and side faces of the openings.

(2) See SINGLE SLOPE CONCRETE BARRIER - JOINT TYPE X CONNECTION FOR SSCB (SPL) plan sheet for segment connection details.

GENERAL NOTES:

The barrier segments shall be connected using Joint Type X. These connections shall be required both for "precast to precast" and for "precast to cast-in-place" barrier segments. (See SINGLE SLOPE CONCRETE BARRIER - JOINT TYPE X CONNECTION FOR SSCB (SPL) plan sheet for details.)

Barrier segments that are adjacent to a bridge end shall be cast-in-place in accordance with the standard sheet SINGLE SLOPE CONCRETE BARRIER, TYPE 2 - SSCB(3)-02. Barrier segments that are less than 30' in length shall, as directed by the Engineer, be cast-in-place in accordance with the standard sheet SINGLE SLOPE CONCRETE BARRIER, TYPE 2 - SSCB(2)-00A. The openings shall be outlined in cast-in-place segments.

All concrete shall be Class H. All SSCB segments shall receive the same surface finish. Exposed edges at top and ends of segment and at the top horizontal edge of the opening shall be chamfered ¾".

All reinforcing steel shall be Grade 60. Epoxy coated reinforcing shall not be used.

With the approval of the Engineer of Record, Welded Wire Fabric, Deformed, may be substituted for the conventional reinforcing shown. If the Welded Wire Fabric, Deformed, option is chosen, shop plans shall be submitted for review and approval prior to commencement of barrier segment fabrication. Welded Wire Fabric, Deformed, shall be in accordance with ASTM A497.

All concrete, reinforcement, joint connections, and installation shall be considered as part of the barrier for payment.

Average weight of barrier is 630 Lb/LF.

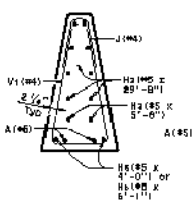

SECTION A-A

Showing reinforcing. X Joint hardware not shown for clarity.

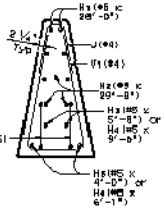

SECTION B-B

Showing reinforcing.

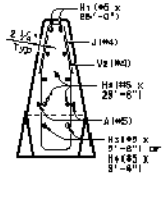

SECTION C-C

Showing reinforcing.

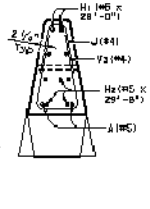

SECTION D-D

Showing reinforcing.

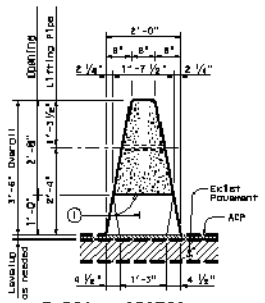

TYPICAL SECTION

Showing structural dimensions. Type X Joint hardware not shown for clarity.

Texas Department of Transportation
Bridge Division

SINGLE SLOPE CONCRETE BARRIER

(WILDLIFE CROSSING) PRECAST SSCB (SPL)

(NOT A STANDARD)
(ONE TIME USE ONLY)

FILE	ssscb91.dgn	DN: TxDOT	CK: GAT	DW: JRP	CK: MVA
©TxDOT MARCH 2005		CONT	SECT	JOB	HIGHWAY
REVISIONS		DIST	COUNTY		SHEET
		PHR			
		DISTRICT	COUNTY	CONTROL	SECT	JOB	HIGHWAY
		CRADDOCK	BOSQUE	0031	01	NTH	SH 144

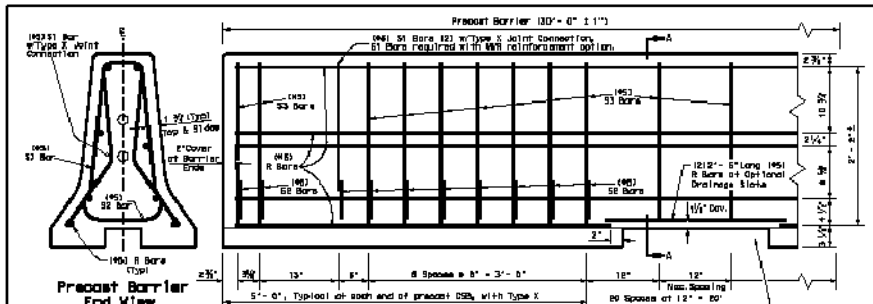

Precast Barrier End View

See CSB(3) Sheet for Joint connection Types

Reinforcement for Precast Concrete Safety Barrier (Type 1)

Showing reinforcement for Joint Type K, See CSB(2) for Joint Types and connection details.

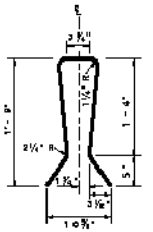

S1 Bar

#5 Rebar (2) (Joint Type K)

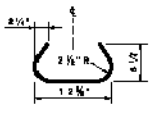

S2 Bar

#5 Rebar(Stirrup) (20) (Joint Type K)

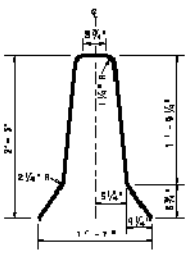

S3 Bar

#3 Rebar

Used with Precast and Cast-in-place Concrete Safety Barrier (CSB).

Note: Two S1 Bars are required with the use of WWR reinforcement option. The S1 Bars may need a slight modification to fit within the WWR apply, as directed by the Engineer.

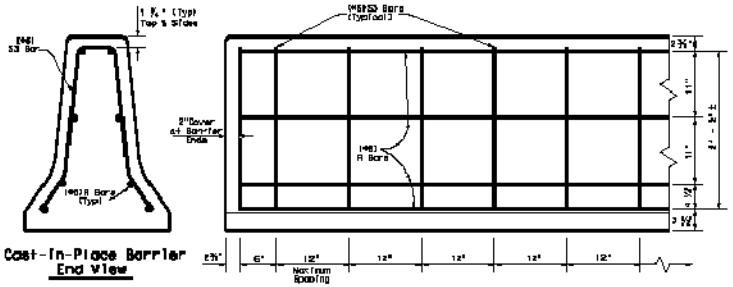

Cast-In-Place Barrier End View

Reinforcement for Cast-in-Place Concrete Safety Barrier (Type 1)

Showing reinforcement for CSB. Expansion joints to be placed every 100 ft. or less.

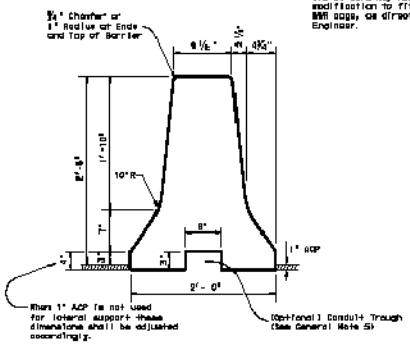

Concrete Safety Barrier

General Notes

1. Concrete shall be Class C or H.
2. Where used, rebar reinforcement shall be Grade 60 and conform to ASTM A615.
3. Precast barrier length shall be 30 ft.
4. Joint connection systems, grout, etc. as shown are considered subsidiary.
5. Conduit trough and drainage slots may be omitted, as shown elsewhere or as directed by the Engineer.
6. Cast-in-place barrier may be slip formed. Additional reinforcement may be tack welded to the upper two-thirds of the reinforcement cage to provide bonding. Do not weld to W bars or anchor bolts.

Approximate Per L.F. Quantities			
		Precast	C.I.P
Concrete	C.Y.	0.108	0.108
Rebar	LB.	17.92	14.00

For Contractor's information only
Weight of one Precast 30 ft. Unit = Approx. 7 Tons

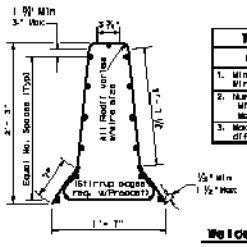

Welded Wire Reinforcement (WWR) Option for Bars S and R (Precast or Cast-in-Place)

Welded Wire Reinforcement (WWR) Table		
DESCRIPTION	LONGITUDINAL WIRE	VERTICAL WIRE
1. Min. Cumulative Total Wire Area	Match R Bars (in^2 /ft.)	Match S Bars (in^2 /ft.)
2. Number of Wires Minimum / Maximum	No. of Wires 6 / 13	(Stirrup ends required at ends of Precast CSB)
3. Maximum wire size differential	The smaller wire shall have an area of 40% or more of the larger wire.	

General Notes

1. Deformed Welded Wire Reinforcement shall conform to ASTM A497.
2. Welded wire cage may require a slight adjustment to accommodate the Type K connection pipes. As directed by the Engineer.
3. Deformed welded wire reinforcement (WWR) may be used as an option to conventional reinforcement. Combinations of reinforcing steel and WWR or configurations of WWR other than shown will be permitted when conditions in the table are satisfied and the dimension from the end of section to first welded wire does not exceed 3".

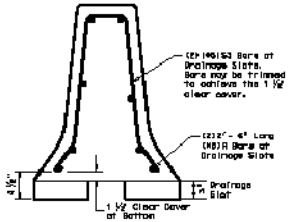

Section A-A

Steel Placement at Drainage Slot (If drainage slots are required)

Texas Department of Transportation
Design Division (Austin)

CONCRETE SAFETY BARRIER (F-SHAPE)

REINFORCEMENT FOR PRECAST AND CAST-IN-PLACE BARRIER (TYPE 1)

CSB(1)-04

FILE: csb01d-04.dgn	DN: TxDOT	CK: JM	DW: BCD	CK:
©TxDOT December 2004	CONT	FEDERAL AID PROJECT		SHEET
REVISIONS	DISTRICT	COUNTY	STATE	JOB	HIGHWAY

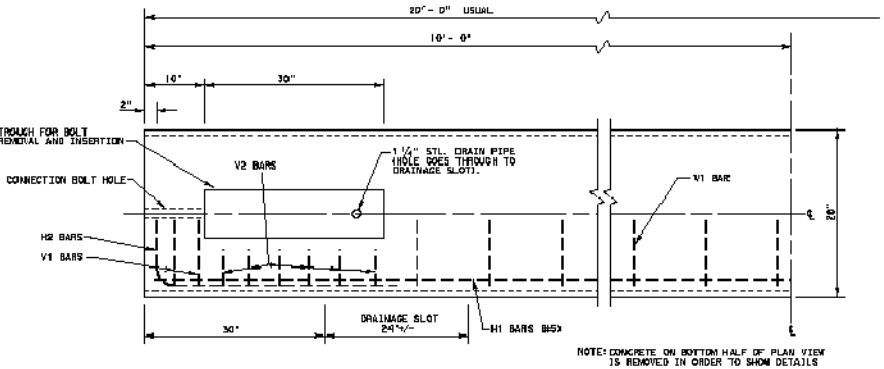

PLAN VIEW - TYPE 1
(SYMMETRICAL ABOUT CENTER LINES)

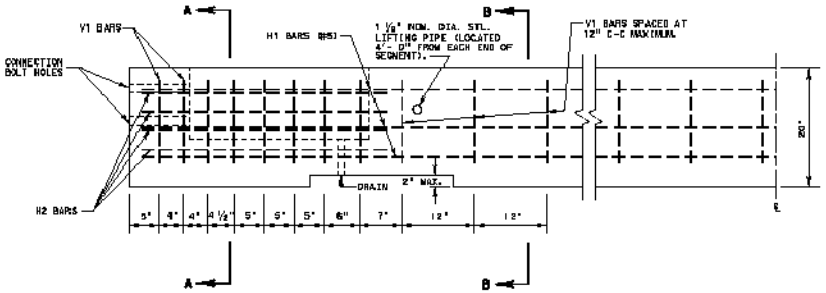

ELEVATION - TYPE 1
(SYMMETRICAL ABOUT CENTER LINES)

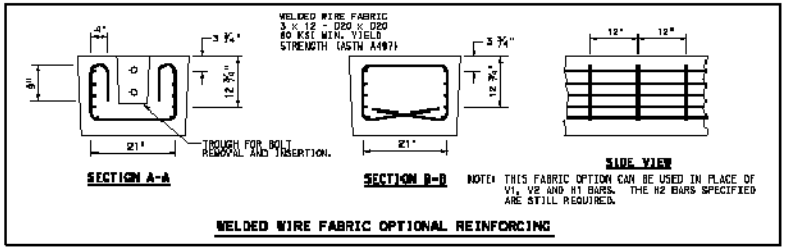

WELDED WIRE FABRIC OPTIONAL REINFORCING

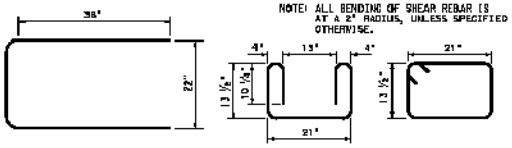

H2 BAR (#5) (GRADE 60 MINIMUM)

V2 BAR (@4)

V1 BAR (#4)

NOTE: H2 REBAR IS TO BE BENT AT A 3" RADIUS.

NOTE: ALL BENDING OF SHEAR REBAR IS AT A 2" RADIUS, UNLESS SPECIFIED OTHERWISE.

REINFORCING STEEL DETAILS

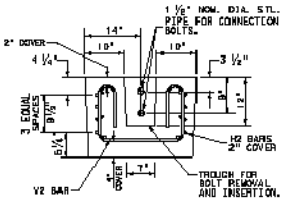

SECTION A-A

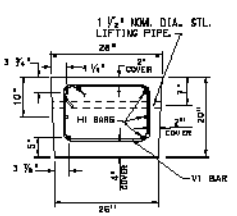

SECTION B-B

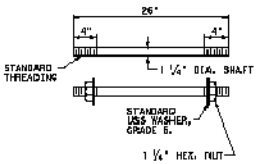

CONNECTION BOLT

FOR CONTRACTORS INFORMATION ONLY

(TYPE 1) APPROX. QUANTITIES PER FT. SECTION		
CONCRETE	CY	2.6
REINFORCING STEEL	LBS	330
TOTAL BARRIER WT.	LBS	11000

GENERAL NOTES

1. BARRIER LENGTH SHALL BE 20 FEET (+/- 1 INCH) UNLESS OTHERWISE SPECIFIED ON THE PLANS.
2. ALL CONCRETE, REINFORCEMENT, ANCHOR BOLTS, BLOCKING, ETC., AS SHOWN ARE CONSIDERED AS PART OF THE BARRIER FOR PAYMENT.
3. ALL CONCRETE SHALL BE CLASS A, C, OR H, UNLESS OTHERWISE SPECIFIED.
4. ALL REINFORCING STEEL SHALL BE GRADE 40, UNLESS OTHERWISE SPECIFIED.
5. CHAMFER ALL EDGES ¾ INCH, AS DIRECTED BY THE ENGINEER.
6. STEEL PIPE SHALL BE HOT DIP GALVANIZED IN CONFORMANCE TO ASTM DESIGNATION A123. BOLTS, NUTS AND WASHERS SHALL BE HOT-DIP GALVANIZED TO ASTM DESIGNATION A153.
7. BOLTS SHALL CONFORM TO ASTM A36. NUTS SHALL CONFORM TO A307 REQUIREMENTS AND SHALL BE TAPPED OR CHASED AFTER GALVANIZING. BOLTS AND NUTS SHALL HAVE CLASS 2A AND 2B FIT TOLERANCES.
8. THE BARRIER SHOULD BE LIGHT IN COLOR AND SHOULD BE SUPPLEMENTED BY DELINEATION AS DETAILED ELSEWHERE IN THE PLANS.

Texas Department of Transportation
Design Division (Roadway)

LOW PROFILE CONCRETE BARRIER
(PORTABLE AND PRECAST)

LPCB(1)-92

SHEET 1 OF 2

FILE: lpcb192.dgn	DN:	CK:	DW:	CK:
©TxDOT SEPTEMBER 1992	CONTROL	PROJECT		SHEET
REVISIONS	COUNTY			

Bibliography

Benson, K. (2004). *Hydraulic Effects of Safety End Treatments on Culvert Performance.* M.S. Thesis in Engineering, The University of Texas at Austin.

Bos, M. (1989). Discharge Measurements Structures. *Publication 20* . Wageningen, The Netherlands: International Institute for Land Reclamation and Improvement.

Charbeneau, R., Henderson, A., & Sherman, L. (2006). Hydraulic Performance Curves for Highway Culverts. *Journal of Hydraulic Engineering , Vol. 132* (No. 5), p. 474-481.

Charbeneau, R., Klenzendorf, B., & Barrett, M. (2008). *Hydraulic Performance of Bridge Rails.* Austin, TX: Center for Transportation Research.

King, H., & Brater, E. (1963). *Handbook of Hydraulics, Fifth Edition.* New York: McGraw-Hill Book Company.

Klenzendorf, J. B. (2007). *Hydraulic Performance of Bridge Rails based on Rating Curves and Submergence Effects.* M.S. Thesis in Engineering, University of Texas at Austin.

Mott, R. (2000). *Applied Fluid Mechanics.* Upper Saddle River, New Jersey: Prentice-Hall, Inc.

Rouse, H. (1950). *Engineering Hydraulics, Proceedings of the Fourth Hydraulics Conference, Iowa Institute of Hydraulic Research, June 12-15, 1949.* New York: John Wiley & Sons, Inc.

TxDOT. (2009). *Roadway Standards.* Retrieved 2009, from Texas Department of Transportation Homepage: http://www.dot.state.tx.us/insdtdot/orgchart/cmd/cserve/standard/rdwylse.htm

Villemonte, J. (1947). Submerged-Weir Discharge Studies. *Engineering News-Record* , 866-869.